Journal of Controlled Release 335 (2021) 21–37

Contents lists available at ScienceDirect

Journal of Controlled Release

journal homepage: www.elsevier.com/locate/jconrel

PEG-polyaminoacid based micelles for controlled release of doxorubicin: Rational design, safety and efficacy study

Silvia Brunato [a], Francesca Mastrotto [a], Federica Bellato [a], Chiara Bastiancich [b], Alessandra Travanut [c], Mariangela Garofalo [a], Giuseppe Mantovani [c], Cameron Alexander [c], Veronique Preat [b], Stefano Salmaso [a,*], Paolo Caliceti [a]

[a] Department of Pharmaceutical and Pharmacological Sciences, University of Padova, via F. Marzolo 5, 35131 Padova, Italy
[b] Université catholique de Louvain, Louvain Drug Research Institute, Advanced Drug Delivery and Biomaterials, Avenue Mounier 73, 1200 Brussels, Belgium
[c] Molecular Therapeutics and Formulations Division, School of Pharmacy, University of Nottingham, University Park, Nottingham NG7 2RD, UK

ARTICLE INFO

Keywords:
Polyaminoacids
Doxorubicin
pH-sensitive drug carriers
Polymeric micelles
Controlled release

ABSTRACT

A library of amphiphilic monomethoxypolyethylene glycol (mPEG) terminating polyaminoacid *co*-polymers able to self-assemble into colloidal systems was screened for the delivery and controlled release of doxorubicin (Doxo). mPEG-Glu/Leu random *co*-polymers were generated by Ring Opening Polymerization from 5 kDa mPEG-NH_2 macroinitiator using 16:0:1, 8:8:1, 6:10:1, 4:12:1 γ-benzyl glutamic acid carboxy anhydride monomer/leucine *N*-carboxy anhydride monomer/PEG molar ratios. Glutamic acid was selected for chemical conjugation of Doxo, while leucine units were introduced in the composition of the polyaminoacid block as spacer between adjacent glutamic repeating units to minimize the steric hindrance that could impede the Doxo conjugation and to promote the polymer self-assembly by virtue of the aminoacid hydrophobicity.

The benzyl ester protecting the γ-carboxyl group of glutamic acid was quantitatively displaced with hydrazine to yield $mPEG_{5kDa}$-b-($hydGlu_m$-*r*-Leu_n). Doxo was conjugated to the diblock *co*-polymers through pH-sensitive hydrazone bond. The Doxo derivatized co-polymers obtained with a 16:0:1, 8:8:1, 6:10:1 Glu/Leu/PEG ratios self-assembled into 30–40 nm spherical nanoparticles with neutral zeta-potential and CMC in the range of 4-7 μM. At pH 5.5, mimicking endosome environment, the carriers containing leucine showed a faster Doxo release than at pH 7.4, mimicking the blood conditions. Doxo-loaded colloidal formulations showed a dose dependent cytotoxicity on two cancer cell lines, CT26 murine colorectal carcinoma and 4T1 murine mammary carcinoma with IC_{50} slightly higher than those of free Doxo. The carrier assembled with the polymer containing 6:10:1 hydGlu/Leu/PEG molar ratio {$mPEG_{5kDa}$-b-[(Doxo-$hydGlu)_6$-*r*-Leu_{10}]} was selected for subsequent *in vitro* and *in vivo* investigations. Confocal imaging on CT26 cell line showed that intracellular fate of the carrier involves a lysosomal trafficking pathway. The intratumor or intravenous injection to CT26 and 4T1 subcutaneous tumor bearing mice yielded higher antitumor activity compared to free Doxo. Furthermore, $mPEG_{5kDa}$-b-[(Doxo-$hydGlu)_6$-*r*-Leu_{10}] displayed a better safety profile when compared to commercially available Caelyx®.

1. Introduction

Nanosized drug delivery systems have emerged as a strategy to enhance the therapeutic performance of anticancer drugs as they improve their biopharmaceutical features and provide for accumulation and release within tumor tissue, thus reducing systemic side effects due to unspecific drug biodistribution [1]. Accordingly, successful results have been obtained with several anticancer drugs loaded in nanosized formulations including liposomes, micelles and nanoparticles [2,3]. For example, liposomal formulation of doxorubicin (Doxo) Doxil®, approved in the US in 1995 for the treatment of ovarian cancer and AIDS-related Kaposi's sarcoma, provided a number of advantages mostly correlated to safety improvement (reduced cardiotoxicity, nausea and vomiting, as well as less myelosuppression), while general consensus has not been reached concerning the increase survival in patients treated with liposomal Doxo compared to the free drug [4]. Therefore, there is still need of systems that can selectively target the disease site and enhance the therapeutic outcome. For such a reason, nanovectors must

* Corresponding author.
E-mail address: stefano.salmaso@unipd.it (S. Salmaso).

https://doi.org/10.1016/j.jconrel.2021.05.010
Received 27 July 2020; Received in revised form 7 May 2021; Accepted 9 May 2021
Available online 11 May 2021

be sharply engineered to yield tailored structures that selectively deliver anticancer drugs to the disease site by active or passive process and release the drug according to controlled mechanisms.

Polyaminoacid-based vectors are emerging as promising drug vehicles due to their high biocompatibility and biodegradability [5]. Indeed, the clearance of the components of drug carriers from the body is a requisite for approval by regulatory agencies and clinical translation of this class of therapeutic systems. Thus, polyaminoacid-based carriers may represent a safer option to develop drug nanocarriers. In addition, depending on their composition, the reactive pendant groups of the side-chain of polyaminoacids, such as aspartic or glutamic acids, can be exploited for the conjugation of drugs or diagnostic agents, or they can be functionalized with stimuli-responsive linkers to endow drug release by tissue and intracellular microenvironmental triggers *e.g.* enzymatic pools, pH, redox potential [6]. Systems exploiting enzymes such as cathepsins, which can cleave polyaminoacid based drug conjugates and are overexpressed in tumor tissues, are under clinical development for local controlled drug release [7]. Additionally, biopharmaceutical features of this class of nanovectors can be properly tailored by tuning the polymer composition. For example, the conjugation of hydrophilic polymers (such as PEG) to hydrophobic polyaminoacids can yield macromolecules that self-assemble into micelles, which provide for high drug loading, prolonged blood circulation, and enhanced passive tumor accumulation by enhanced permeation and retention (EPR) effect [8–12]. However, the hydrophobic/hydrophilic balance of PEG-polyaminoacid *block-co*-polymers must be sharply optimized, as it dictates the stability of the micelles in biological environments, as well as the release of physically encapsulated or chemically conjugated drug molecules. The chemical and physical drug loading in the polymeric micelles may offer the opportunity for combination therapy further expanding the versatility and therapeutic potential of these systems [13].

In this work, we generated a library of amphiphilic di-block *co*-polymers composed by a hydrophilic block of methoxypolyethylene glycol (mPEG) and a polyaminoacid block with different ratios of glutamic acid-γ-hydrazide (hydGlu) and leucine (Leu), to investigate the polymer structure/drug loading relationship and efficiency of drug delivery to the tumor while reducing systemic drug exposure [14].

While drug delivery systems reported in the literature derive from rather sophisticated conceptualization in response to the complexity of tumor, we explored here a rational approach to achieve high drug loading in the carrier, efficient drug delivery to the tumor with reduced systemic Doxo exposure using biodegradable and non-toxic materials. The antitumor efficacy and safety profile of selected micellar formulations was estimated comparatively using two solid subcutaneous tumor models, CT26 colorectal carcinoma and 4T1 breast tumor, with that of a commercially available liposomal formulation of Doxo.

2. Materials and methods

5.0 kDa methoxy-polyethyleneglycol ($mPEG_{5kDa}$-OH) was purchased from Sigma-Aldrich (St. Louis, USA). All the other chemical reagents including salts and analytical grade solvents were purchased from Sigma-Aldrich (St. Louis, MO, USA), VWR (Milan, Italy) or Carlo Erba (Milan, Italy). $mPEG_{5kDa}$-OH was azeotropically dried with toluene under reduced pressure prior to use, while all other products were used without further purification. Doxo hydrochloride was purchased from LC laboratories (Woburn, MA, USA). The water used for the preparation of solutions was "ultrapure" water (milliQ-grade, 0.06 μS cm^{-1}), produced with a Millipore Milli-Q purification system (Burlington, MA, USA). Dialysis membranes with a molecular weight cut off (MWCO) of 3.5–5 kDa and Flot-a-Lyzers with MWCO 3.5–5 kDa were purchased from Prodotti Gianni (Milan, Italy).

All the media and materials used for cell culture were obtained from Gibco (Life Technologies, Waltham, MA, USA), including phosphate buffered saline (PBS), RPMI 1640 Medium, Fetal Bovine Serum (FBS), Penicillin G sodium and Streptomycin sulfate. 4′,6-diamidino-2-phenylindole dihydrochloride (DAPI), 3-(4,5-dimethylthiazol-2-yl)-2,5-diphenyltetrazolium bromide (MTT), Corning® T-75 culture flasks, Rat Serum and Triton® X-100 were purchased from Sigma-Aldrich (St. Louis, MO, USA). Rat anti-mouse CD107a (LAMP-1) and chicken anti-rat IgG(H + L) cross-adsorbed secondary antibody Alexa Fluor 488 conjugated were obtained by Thermoscientific (Waltham, MA, USA).

CT26 colon carcinoma cell line and 4T1 breast carcinoma cell line were purchased from ATCC cell bank (Manassas, VA, USA). Six-weeks old BALB/c female mice were provided by Janvier Labs (Le Genest-St-Isle, France).

2.1. Synthesis of $mPEG_{5kDa}$-NH_2

2.1.1. Synthesis of $mPEG_{5kDa}$-allyl carbamate

$mPEG_{5kDa}$-OH (20.0 g, 4.02 mmol) was dissolved in chloroform (15 mL) and added of allyl isocyanate (1.30 g, 15.6 mmol) and triethylamine (2.80 mL, 2.02 g, 20.0 mmol). The mixture was maintained under stirring at room temperature for 18 h. The polymer was isolated by precipitation in diethyl ether (40 mL), centrifuged at 5000 rpm for 5 min, rinsed three times with diethylether (40 mL) and finally dried under reduced pressure. $mPEG_{5kDa}$-allyl carbamate (19.5 g, 3.82 mmol) was obtained as a white solid in 95% yield. The product was analyzed by ^{1}H NMR and MALDI-ToF mass spectroscopy using SuperDHB as the matrix.

MALDI-ToF spectrum showed the expected set of signals for the Na^+ and K^+ adducts of $mPEG_{5kDa}$ allyl carbamate. Using the chains with 110 oxyethylene repeating units as a representative example - $C_{225}H_{449}NO_{112}Na^+$: theor. 4981.0, found 4980.8; $C_{225}H_{449}NO_{112}K^+$: theor. 4996.9, found 4996.9. Complete spectrum is shown in Fig. SI-1 (Supplementary Information).

^{1}H NMR (400 MHz, $CDCl_3$): δ 5.82 (m, 1H, CH═CH_2), 5.21 (dq, J = 17.1, 1.6 Hz, 1H, CH═CH*H*, 5.13 (dq, J = 10.2, 1.4 Hz, 1H, CH═C*H*H, 4.97 (bs, 1H, (C═O)N*H*), 4.22 (m, 2H, -CH_2OC(O)), 3.63 (s, 476H, −(OCH_2CH_2)$_n$), 3.36 (s, 3H, CH_3O-).

2.1.2. Synthesis of $mPEG_{5kDa}$-NH_2

$mPEG_{5kDa}$-allyl carbamate (10.1 g, 1.99 mmol) was solubilized in methanol (10 mL). Cysteamine hydrochloride (1.13 g, 9.95 mmol) and 2,2′-dimethoxy-2-phenylacetophenone (DPAP) (0.102 g, 0.400 mmol) were dissolved in 2 mL and 1 mL of methanol, respectively, and then sequentially added to the $mPEG_{5kDa}$-allyl carbamate solution. The final mixture was aliquoted in vials and irradiated with UV light (λ = 350 nm, 36 W) for 3 h. When allyl signals could no longer be detected by ^{1}H NMR, the aliquots were pulled together, and methanol was removed under vacuum. The resulting residue was solubilized in water (100 mL) and extracted 3 times with ethyl acetate (100 mL) to remove organic species deriving from the decomposition of DPAP. Next, the aqueous phase was extracted 2 times with a 3:1 vol:vol dichloromethane: isopropanol (100 mL) and the organic phase was dried under reduced pressure to obtain the $mPEG_{5kDa}$-cysteamine ($mPEG_{5kDa}$-NH_2) as white powder (9.95 g, 1.92 mmol), (98% yield). MALDI-TOF analysis of $mPEG_{5kDa}$-NH_2 was performed using SuperDHB as a matrix.

MALDI-ToF spectrum showed the expected set of signals for the H^+, Na^+ and K^+ adducts of this polymer. Using the chains with 110 oxyethylene repeating units as a representative example - $C_{227}H_{456}N_2O_{112}S^-H^+$: theor. 5036.0, found 5035.8; $C_{227}H_{456}N_2O_{112}S^-Na^+$: theor. 5058.0, found 5057.9; $C_{227}H_{456}N_2O_{112}S^-K^+$: theor. 5073.9, found 5073.8. Complete spectrum is shown in Fig. SI-1.

SEC analysis (DMF + 0.1% LiBr): $M_{n,SEC}$ = 7.3 kDa; Đ = 1.09.

^{1}H NMR (400 MHz, $CDCl_3$): δ 4.22 (m, 2H, -CH_2OC(O)), 3.63 (m, 476H, −(OCH_2CH_2)$_n$), 3.37 (s, 3H, CH_3O), 3.29 (q, J = 5.9 Hz, 2H, (O)CNHCH_2), 3.17 (bs, 2H, CH_2NH_2), 2.94 (t, J = 7.3 Hz, 2H, SCH_2CH$_2$NH_2), 2.63 (t, J = 7.1 Hz, 2H, CH$_2$ CH$_2$CH_2S), 1.90 (m, 2H, CH_2CH$_2$S).

2.2. Synthesis of γ-benzyl-glutamic acid N-carboxyanhydride (BnOGlu-NCA)

The protocol for γ-benzyl-glutamic acid NCA synthesis was adapted from Markland et al. [15] and Williams et al. [16] γ-benzyl-glutamic acid (19.9 g, 83.8 mmol) was suspended in tetrahydrofuran (THF, 200 mL). α-pinene (33.0 mL; 20.9 mmol) and solid triphosgene (9.14 g, 30.8 mmol) were sequentially added to the suspension under nitrogen atmosphere. The resulting mixture was heated under reflux at 56 °C until the suspension turned yellow and clear (90 min). The solution was then cooled down to room temperature and bubbled with nitrogen for 4 h to remove gaseous co-product and potential traces of unreacted phosgene. An aqueous 1 M NaOH trap was connected to the system during this procedure to neutralize the gaseous species removed from the reaction mixture. The solution was then concentrated to ~70 mL under reduced pressure, and petroleum ether was added (50 mL). The resulting solution was transferred into a conical flask, sealed, and left to crystallize at −18 °C overnight. γ-benzyl-glutamic acid NCA (16.3 g, 61.7 mmol) was isolated by filtration in 82% yield.

^{1}H NMR (400 MHz, $CDCl_3$): δ 7.35 (m, 5H, C*H* aromatic), 6.64 (s, 1H, N*H*CH), 5.14 (s, 2H, OCH_2Ph), 4.38 (t, J = 6.1 Hz, 1H, NHC*H*), 2.59 (t, J = 6.9 Hz, 2H, CH_2C(O)), 2.26 (m, 1H, CHC*H*H), 2.13 (m, 1H, CHCH*H*).

^{13}C NMR (101 MHz, $CDCl_3$): δ 172.52 (1C, *C*(*O*)CH), 169.48 (1C, *C*(*O*)O), 151.97 (1C, *C*(*O*)NH), 135.35 (1C, C aromatic), 128.85 (2C, CH aromatic), 128.73 (2C, CH aromatic), 128.50 (1C, CH aromatic), 67.25 (1C, OCH_2Ph), 57.07 (1C, *C*HCH$_2$), 29.98 (1C, CH$_2$CH_2), 27.05 (1C, *C*H$_2$CH$_2$).

FT-IR: υ 3247, 2320, 1862, 1772, 1718, 1493, 1396, 1251, 1183, 1110, 796, 961 cm^{-1}.

2.3. Synthesis of leucine N-carboxyanhydride (Leu-NCA)

This NCA monomer was prepared as described by Smeets et al. [17]. Leucine (8.02 g, 61.0 mmol) was suspended in anhydrous THF (100 mL). α-pinene (25.0 mL, 157 mmol) and solid triphosgene (6.70 g, 22.2 mmol) were sequentially added under nitrogen atmosphere. The suspension was heated under reflux at 64 °C until it turned yellow and clear (~ 30 min). The solution was then cooled down to room temperature and bubbled with nitrogen following the same procedure described above for the synthesis of γ-benzyl-glutamic acid NCA. The solvent was then removed under reduced pressure to yield a yellow oily residue. Petroleum ether (300 mL) was added to induce the precipitation of Leu-NCA as a white solid. This precipitate was filtered, washed with ice-cold petroleum ether (3 × 25 mL), and dried under reduced pressure, to give leucine *N*-carboxyanhydride (Leu-NCA) as a white solid (7.65 g, 48.6 mmol) with a recovery yield of 95% (mol/mol).

^{1}H NMR (400 MHz, $CDCl_3$): δ 6.43 (bs, 1H, N*H*CH) 4.33 (dd, J = 8.9, 4.0 Hz, 1H, NHC*H*), 1.82 (m, 2H, CH_2CH), 1.68 (m, 1H, C*H*(CH$_3$)$_2$), 0.99 (m, 6H, CH(CH_3)$_2$).

^{13}C NMR (101 MHz, $CDCl_3$): δ 170.25 (1C, *C*(*O*)CH), 153.38 (1C, *C*(*O*)NH), 56.33 (1C, *C*HCH$_2$), 40.88 (1C, *C*H$_2$CH), 25.06 (1C, *C*H(CH$_3$)$_2$), 22.79 and 21.59 (2C, CH(*C*H$_3$)$_2$).

FT-IR: υ 2960, 1798, 1750, 1468, 1117, 1079 cm^{-1}.

2.4. Synthesis of mPEG$_{5kDa}$-b-(BnOGlu$_m$-r-Leu$_n$) random co-polymers

This procedure was adapted from the protocol reported by Zhao et al. [18]. The mPEG$_{5kDa}$-b-(BnOGlu$_m$-*r*-Leu$_n$) *co*-polymer library was synthetized by Ring Opening Polymerization (ROP) using mPEG$_{5kDa}$-NH$_2$ as the initiator, and Glu-NCA and Leu-NCA as the monomers at different relative molar ratios. For the synthesis of the *co*-polymer library, the amount of monomers to be used was calculated considering targeted monomer conversions of 90% and 70% for Glu-NCA and Leu-NCA (Leu-NCA was found to react more slowly than Glu-NCA in these co-polymerization reactions), respectively, based on preliminary polymerization studies (Data not shown).

2.4.1. Representative example: synthesis of mPEG$_{5kDa}$-b-(BnOGlu$_8$-r-Leu$_8$)

mPEG$_{5kDa}$-NH$_2$ (0.500 g, 0.0970 mmol) was dissolved in toluene (10 mL), and the solvent was removed under reduced pressure to azeotropically eliminate traces of moisture in the initial mPEG$_{5kDa}$-NH$_2$ starting material. Anhydrous DMF (12 mL) was added to mPEG$_{5kDa}$-NH$_2$ under argon atmosphere, the flask was sonicated for five minutes to completely solubilize the macroinitiator, then the resulting solution was degassed by argon bubbling for 30 min. For the synthesis of mPEG$_{5kDa}$-b-(BnOGlu$_8$-*r*-Leu$_8$), Glu-NCA (0.255 g, 0.871 mmol) and Leu-NCA (0.183 g, 1.16 mmol) were poured into a round-bottomed flask under argon atmosphere, then the mPEG$_{5kDa}$-NH$_2$ initiator solution was added *via* cannula, to give a mPEG$_{5kDa}$-NH$_2$:BnOGlu:Leu feed ratio of 1:9:12, and the resulting mixture was stirred at room temperature. The reaction solution was bubbled with argon twice a day for 30 min. After 7 days the mixture was added dropwise under stirring to 100 mL of Et$_2$O, and the resulting suspension centrifuged for five minutes at 5000 rpm. The supernatant was discarded, the precipitate was dissolved in CH_2Cl_2 (5 mL) and then the side products, consisting in poly(BnOGlu$_m$-*r*-Leu$_n$) oligomers were precipitated in methanol. After centrifugation for 5 min at 5000 rpm, the supernatant was recovered and dropwise added to 100 mL of Et$_2$O to isolate, after filtration, mPEG$_{5kDa}$-b-(BnOGlu$_8$-*r*-Leu$_8$) as a white solid. The precipitate was dried for 24 h under reduced pressure to remove traces of solvents, then characterized by ^{1}H NMR and SEC.

mPEG$_{5kDa}$-b-(BnOGlu$_8$-*r*-Leu$_8$) ^{1}H NMR (400 MHz, $CDCl_3$): δ 7.28 (m, 40H, C*H* aromatic), 5.02 (s, 16H, CH_2Ph), 4.01 (m, 16H, C(*O*)C*H*, C(*O*)C*H*NH$_2$), 3.64 (s, 476H, −(OCH_2CH_2)$_n$), 3.38 (s, 3H, CH_3O), 2.70–2.17 (m, 58H, NH(CH_2)$_3$S(CH_2)$_2$, CH_2CH_2C(O), CH_2CH(CH$_3$)$_2$), 0.86 (m, 48H, CH(CH_3)$_2$). SEC analysis (DMF + 0.1% LiBr): M_n = 10.5 kDa; Đ = 1.11.

Yield of purification process 75% (mol/mol).

2.4.2. mPEG$_{5kDa}$-BnOGlu$_{16}$

mPEG$_{5kDa}$-NH$_2$ (2.00 g, 0.387 mmol), BnOGlu-NCA (1.78 g, 6.77 mmol, 17.5 eq), DMF (41 mL). After 5 days additional BnOGlu-NCA (1.12 g, 4.25 mmol, 11 eq) were added, and the reaction stopped at day 7. ^{1}H NMR (400 MHz, $CDCl_3$): δ 7.43–7.14 (m, 80H, C*H* aromatic), 5.02 (s, 32H, CH_2Ph), 4.19–3.92 (m, 16H, C(*O*)C*H*), 3.64 (s, 476H, (OCH_2CH_2)$_n$), 3.38 (s, 3H, CH_3O), 2.62–2.26 (m, 74H, NH(CH_2)$_3$S(CH_2)$_2$, CH_2CH_2C(O). SEC analysis (DMF + 0.1% LiBr): M_n = 12.2 kDa; Đ = 1.07. Yield of purification process 75% (mol/mol).

2.4.3. mPEG$_{5kDa}$-b-(BnOGlu$_6$-r-Leu$_{10}$)

mPEG$_{5kDa}$-NH$_2$ (2.00 g, 0.387 mmol), BnOGlu-NCA (1.02 g, 4.26 mmol, 10 eq), Leu-NCA (1.27 g, 8.13 mmol, 21 eq), DMF (73 mL). After 5 days additional BnOGlu-NCA (1.32 g, 13 eq) and Leu-NCA (1.03 g, 17 eq) were added, and the reaction stopped at day 7. ^{1}H NMR (400 MHz, $CDCl_3$): δ 7.32 (m, 30H, C*H* aromatic), 5.03 (s, 18H, CH_2Ph), 4.02 (m, 16H, C(*O*)C*H*, C(*O*)C*H*NH$_2$), 3.64 (s, 476H, −(OCH_2CH_2)$_n$), 3.38 (s, 3H, CH_3O), 2.71–2.17 (m, 54H, NH(CH_2)$_3$S(CH_2)$_2$, CH_2CH_2C(O), CH_2CH(CH$_3$)$_2$), 0.88 (m, 60H, CH(CH_3)$_2$). SEC analysis (DMF + 0.1% LiBr): M_n = 10.4 kDa; Đ = 1.09. Yield of purification process 72% (mol/mol).

2.4.4. mPEG$_{5kDa}$-b-(BnOGlu$_4$-r-Leu$_{12}$)

mPEG$_{5kDa}$-NH$_2$ (2.00 g, 0.387 mmol), BnOGlu-NCA (0.713 g, 2.71 mmol, 7 eq), Leu-NCA (1.58 g, 10.1 mmol, 26 eq), DMF (75 mL). After 5 days additional BnOGlu-NCA (0.682 g, 7 eq) and Leu-NCA (1.09 g, 18 eq) were added, and the reaction stopped at day 7. ^{1}H NMR (400 MHz, $CDCl_3$): δ 7.32 (m, 20H, C*H* aromatic), 5.03 (s, 8H, CH_2Ph), 4.02 (m, 16H, C (O)C*H*, C(*O*)C*H*NH$_2$), 3.64 (s, 476H, (OCH_2CH_2)$_n$), 3.38 (s, 3H, CH_3O), 2.72–2.17 (m, 50H, NH(CH_2)$_3$S(CH_2)$_2$, CH_2CH_2C (O), CH_2CH(CH$_3$)$_2$), 0.89 (m, 72H, CH(CH_3)$_2$). SEC analysis (DMF + 0.1% LiBr): M_n = 9.9 kDa; Đ = 1.08. Yield of purification process 77% (mol/mol).

2.5. Synthesis $mPEG_{5kDa}$-b-[(γ-hydrazide-glutamic acid)$_m$-r-leucine$_n$] [$mPEG_{5kDa}$-b-(hydGlu$_m$-r-Leu$_n$)]

The protocol of polymer deprotection was adapted from Bae et al. [11] $mPEG_{5kDa}$-b-(BnOGlu$_8$-*r*-Leu$_8$) (0.500 g, 0.0639 mmol, 0.511 mmol of benzyl ester units) was dissolved in toluene (10 mL) and the solvent was removed under reduced pressure to azeotropically remove moisture. Anhydrous DMF (3.5 mL) was then added to the solution under argon atmosphere, followed by dropwise addition of hydrazine hydrate (0.631 g, 19.7 mmol). The reaction was carried out at 40 °C under stirring for 48 h. The resulting gel-like solution was diluted with additional 3.5 mL of DMF to decrease viscosity. The resulting solution was precipitated in Et_2O (100 mL) and the white solid was isolated by centrifugation. Then, the product was re-dissolved in milliQ water (50 mL) and purified by dialysis (MWCO 3.5 kDa) for two days using 5 L of deionized water as receiving medium. The polymer containing solution was freeze-dried to obtain $mPEG_{5kDa}$-b-(hydGlu$_8$-*r*-Leu$_8$) as a white solid (0.389 g, 0.0470 mmol, 74% mol/mol yield). The γ-hydrazide Glu:Leu monomer ratio was estimated by ^{1}H NMR. The number of hydrazide groups per polymer chain was calculated according to the modified Snyder's assay for the evaluation of hydrazides [19] (λ = 500 nm, calibration curve: y = 11.997× – 0.0318. R^2 = 0.9982), and the iodine assay for PEG detection [20] (λ = 535 nm, calibration curve: y = 0.0229× + 0.0207. R^2 = 0.9933).

^{1}H NMR (400 MHz, DMSO-d_6): δ 4.16 (m, 16H, C(*O*)C*H*, C(*O*)C*H*NH$_2$), 3.51 (s, 476H, – (OCH_2CH_2)$_n$), 3.24 (s, 3H, CH_3O), 2.05–1.45 (m, 58H, NH(CH_2)$_3$S(CH_2)$_2$, CH_2CH_2C(O), CH_2CH(CH$_3$)$_2$), 0.86 (m, 48H, CH(CH_3)$_2$). SEC analysis (DMF + 0.1% LiBr): M_n = 8.9 kDa; Đ = 1.25. Number of hydrazides per polymer chain: 8.3.

The same procedure was applied to deprotect the other polymers of the library and generate $mPEG_{5kDa}$-hydGlu$_{16}$, $mPEG_{5kDa}$-b-(hydGlu$_6$-*r*-Leu$_{10}$), $mPEG_{5kDa}$-b-(hydGlu$_4$-*r*-Leu$_{12}$).

$mPEG_{5kDa}$-hydGlu$_{16}$: ^{1}H NMR (400 MHz, D_2O): δ 4.34 (m, 16H, C(*O*)C*H*), 3.74 (s, 476H, (OCH_2CH_2)*n*), 3.42 (s, 3H, CH_3O-), 2.75–1.81 (m, 74H, NH(CH_2)$_3$S(CH_2)$_2$, CH_2CH_2C(O). SEC analysis (DMF + 0.1% LiBr): M_n = 12.2 kDa; Đ = 1.03.

Number of hydrazide per polymer chain: 16.1. Yield of purification process 68% (mol/mol) (0.326 g, 0.0424 mmol).

$mPEG_{5kDa}$-b-(hydGlu$_6$-*r*-Leu$_{10}$): ^{1}H NMR (400 MHz, DMSO-d_6) δ 4.16 (m, 16H, (C=O)C*H*, (C=O)C*H*NH$_2$), 3.51 (s, 476H, (OCH_2CH_2)$_n$), 3.24 (s, 3H, CH_3O-), 2.05–1.45 (m, 54H, NH(CH_2)$_3$S(CH_2)$_2$, CH_2CH_2C(O), CH_2CH(CH$_3$)$_2$), 0.87 (m, 60H, CH(CH_3)$_2$). SEC analysis (DMF + 0.1% LiBr): Mn = 8.8 kDa; Đ = 1.15. Number of hydrazide per polymer chain: 6.3. Yield of purification process 75% (mol/mol) (0.354 g, 0.0495 mmol).

$mPEG_{5kDa}$-b-(hydGlu$_4$-*r*-Leu$_{12}$): ^{1}H NMR (400 MHz, DMSO-d_6) δ 4.07 (m, 16H, C(*O*)C*H*, C(*O*)C*H*NH$_2$), 3.51 (s, 476H, (OCH_2CH_2)$_n$), 3.24 (s, 3H, CH_3O), 2.02–1.43 (m, 50H, NH(CH_2)$_3$S(CH_2)$_2$, CH_2CH_2C(O), CH_2CH(CH$_3$)$_2$), 0.87 (m, 72H, CH(CH_3)$_2$). SEC analysis (DMF + 0.1% LiBr): M_n = 9.8 kDa; Đ = 1.20. Number of hydrazide per polymer chain: 4.2. Yield of purification process 70% (mol/mol) (0.336 g, 0.0474 mmol).

2.6. Synthesis and self-assembly of $mPEG_{5kDa}$-b-[(Doxo-hydGlu)$_n$-r-Leu$_m$]

Conjugation of Doxo to $mPEG_{5kDa}$-b-(hydGlu$_8$-*r*-Leu$_8$) was performed using a protocol adapted from Bae et al. [11] $mPEG_{5kDa}$-b-(hydGlu$_8$-*r*-Leu$_8$) (0.300 g; 0.0416 mmol) was dissolved in an anhydrous 1:2 MeOH: DMSO mixture (4.5 mL). Doxo hydrochloride (Doxo-HCl) (0.386 g, 0.666 mmol) was solubilized in 1.5 mL of anhydrous DMSO. The two solutions were mixed and trifluoroacetic acid (TFA) (51 μL, 0.666 mmol) was added as a catalyst. The reaction mixture was left under stirring in the dark at room temperature for three days. The solution was then dropwise added to Et_2O (40 mL) and the red pellet was recovered by centrifugation (5000 rpm, 5 min). This process was repeated 4 times and the product was then desiccated under reduced pressure. To remove the unreacted Doxo, the obtained red powder was dissolved in 1:1 *v*/v DMSO:[10 mM Phosphate buffer, pH 7.8 (PB)] mixture, transferred into a 3.5–5 kDa MWCO dialysis bag and dialyzed against the same solvent mixture for 24 h, replacing the solvent four times. The presence of the unreacted drug was monitored by thin layer chromatography (TLC) run with MeOH after slides preconditioning with 5% *v*/v triethylamine (TEA) in MeOH. Dialysis was carried out until complete disappearance of free Doxo in the dialysis bag solution. Afterwards, the composition of the dialysis medium was gradually varied from a 1:1 to 0:1 v/v DMSO: PB ratio in six hours to remove the organic solvent and to induce the self-assembling of the polymer-drug conjugates. Finally, the dialysis medium was changed to deionized water (DI water) adjusted to pH 7.8 with ammonia and dialyzed for further three hours to remove salts. As a control of the assembling behavior, the same dialysis procedure was performed on drug free polymers, in order to evaluate the assembly of micelles in absence of the linked drug. The polymeric self-assembled micelle suspension was then freeze-dried and stored at −20 °C until reconstitution, which was performed by dissolving micelle powders in the required solvent and stirred for three hours on an orbital shaker.

The conjugation yield was assessed by calculating the number of Doxo molecules per polymer chain. The drug/polymer chain molar ratio was estimated according to the spectrophotometric absorbance of the conjugated drug at λ = 488 nm in PB (calibration line: y = 10.416× + 0.0196, R^2 = 0.9991), and the iodine assay for PEG detection [20] (λ = 535 nm, calibration curve: y = 0.0204× – 0.0052, R^2 = 0.9918). The same protocol was used to conjugate Doxo to $mPEG_{5kDa}$-hydGlu$_{16}$, $mPEG_{5kDa}$-b-(hydGlu$_6$-*r*-Leu$_{10}$), $mPEG_{5kDa}$-b-(hydGlu$_4$-*r*-Leu$_{12}$).

$mPEG_{5kDa}$-(Doxo-hydGlu)$_{16}$.

Conjugation yield 44% (mol/mol), 7.0 Doxo molecules/polymer chain.

Doxo content: 32% (*w*/w).

$mPEG_{5kDa}$-b-[(Doxo-hydGlu)$_8$-*r*-Leu$_8$].

Conjugation yield 70% (mol/mol), 5.6 Doxo molecules/polymer chain.

Doxo content: 29% (w/w).

$mPEG_{5kDa}$-b-[(Doxo-hydGlu)$_6$-*r*-Leu$_{10}$].

Conjugation yield 88% (mol/mol), 5.3 Doxo molecules/polymer chain.

Doxo content: 28% (w/w).

$mPEG_{5kDa}$-b-[(Doxo-hydGlu)$_4$-*r*-Leu$_{12}$].

Conjugation yield 100% (mol/mol), 4.0 Doxo molecules/polymer chain.

Doxo content: 23% (w/w).

2.7. Critical micelle concentration (CMC)

2.7.1. CMC by pyrene assay for $mPEG_{5kDa}$-b-(hydGlu$_m$-r-Leu$_n$)

The protocol by Ambrosio et al. [21] was adapted to assess the CMC of the drug-free *co*-polymers $mPEG_{5kDa}$-b-(hydGlu$_m$-*r*-Leu$_n$). 20 μL aliquots of a 5 mg/mL pyrene solution in acetone were transferred in vials and the organic solvent was removed under reduced pressure. Then, 1 mL of $mPEG_{5kDa}$-hydGlu$_m$-*r*-Leu$_n$ in 10 mM phosphate buffer, 0.15 M NaCl, pH 7.4 in the 0–300 μM range was added to each vial and stirred overnight on an orbital shaker, in the dark at room temperature. Each sample was prepared in triplicate. Afterwards, the samples were centrifuged three times at 13,000 rpm for 3 min, and the supernatants were analyzed by fluorescence spectroscopy with an excitation wavelength of 335 nm and recording the emission spectra from 350 to 450 nm. The ratio between the emission intensities at 384 nm (I_3) and 373 nm (I_1), I_3/I_1, was plotted *vs* the polymer logarithmic concentration. The CMC value was derived from the cross-point of the two straight lines fitting through the points [22,23].

2.7.2. CMC by spectrofluorimetric analysis and DLS for $mPEG_{5kDa}$-b-[(Doxo-hydGlu)$_m$-r-Leu$_n$]

1 mL of 0–50 μM of $mPEG_{5kDa}$-b-[(Doxo-hydGlu)$_m$-*r*-Leu$_n$] in 10 mM

phosphate buffer, 0.15 M NaCl, pH 7.4 was prepared and stirred overnight on an orbital shaker in the dark at room temperature. Each sample was prepared in triplicate. Then, the samples were analyzed by fluorescence spectroscopy using an excitation wavelength of 490 nm and recording the emission spectra in the λ = 510–600 nm range. The emission intensities at λ = 555 nm was plotted *vs* the polymer concentration and the CMC was derived from the cross-point of the two lines fitting the points of the increasing fluorescence intensity with that fitting the points of decreasing fluorescent intensity.

The same samples were analyzed by Malvern Dynamic Light Scattering Zetasizer Ultra (Malvern, UK) equipped with optical fluorescence filter wheel. The derived mean count rate was plotted *vs* the polymer logarithmic concentrations. The CMC value were obtained from the cross-point of the two straight lines fitting through the points.

2.8. Size and zeta potential analysis

The particle size, size distribution and zeta potential were measured by using a Malvern Dynamic Light Scattering Zetasizer Nano (Malvern, UK) equipped with a red laser (λ = 633 nm) at a fixed angle of 173° at 25 °C. DTS applications 6.12 software was used for the data analysis. The particle size and size distribution were determined by using 100 μM $mPEG_{5kDa}$-b-$(hydGlu_m$-*r*-$Leu_n)$ and $mPEG_{5kDa}$-b-$[(Doxo\text{-}hydGlu)_m$-*r*-$Leu_n]$ colloidal suspensions in 10 mM phosphate, 150 mM NaCl, pH 7.4 (PBS). Analyses were performed soon after micelle preparation and after 3 min centrifugation at 3000 rpm. The size values were reported as volume, number and intensity. The zeta-potential was obtained by using 100 μM $mPEG_{5kDa}$-b-$(hydGlu_m$-*r*-$Leu_n)$ and $mPEG_{5kDa}$-b-$[(Doxo\text{-}hydGlu)_m$-*r*-$Leu_n]$ colloidal suspensions in 10 mM HEPES. For each sample, DLS measurements were performed in triplicate with 10 runs per 10-s measurement.

Stability of micelles over time was assessed by DLS analysis. Colloidal dispersions of $mPEG_{5kDa}$-b-$(hydGlu_m$-*r*-$Leu_n)$ and $mPEG_{5kDa}$-b-$[(Doxo\text{-}hydGlu)_m$-*r*-$Leu_n]$ in PBS, pH 7.4 or 10 mM sodium acetate, 150 mM NaCl, pH 5.5 were prepared as reported above and added of 2.5% *v/v* FBS to a final micelle concentration of 100 μM. The samples were incubated at 37 °C and analyzed by DLS at scheduled time.

2.9. Transmission electron microscopy

10 μL drop of a 100 μM polymeric micelles in MilliQ water were placed on a homemade carbon coated copper grid, and the solvent was allowed to dry at room temperature. Then, the samples were treated with 1% uranyl acetate in distilled water for 5 min at room temperature to provide for negative staining. Transmission electron microscopy analyses were carried out using a FEI Tecnai G2 microscope (Hillsboro, OR, USA). Particle size analysis was performed with ImageJ Software (developed at the National Institute of Health, Bethesda, MD, USA). The average size of the polymeric colloidal systems was calculated by measuring 50 individual particles with ImageJ software version 1.51j8 (National Institutes of Health software package by Wayne Rasband; Bethesda, MD, USA) and particle size distribution histograms were generated.

2.10. Release studies

Solutions of free Doxo and Doxo-conjugated polymeric micelles in PBS were diluted at a Doxo equivalent concentration of 400 μM in PBS, pH 7.4, or 10 mM sodium acetate, 150 mM NaCl, pH 5.5. The Doxo equivalent concentration was selected to yield a *co*-polymer concentration about 10 times higher than that of the conjugate with the highest CMC of the conjugates (6.7 μM for $mPEG_{5kDa}$-$(Doxo\text{-}hydGlu)_{16}$. Aliquots (1.5 mL) of these solutions were transferred into a Float-A-Lyzer® G2 system, 3.5–5 kDa MWCO, and dialyzed against the same buffer (500 mL) thermostatted with a water bath at 37 °C under stirring. At fixed time points, the concentration of Doxo inside the Float-A-Lyzer® G2 system was assessed by sampling 20 μL of the solution and tested by spectrophotometric analysis (λ_{max} 488 nm) using a calibration line ($y = 10.416\times + 0.0196$, $R^2 = 0.9991$) and molar extinction coefficient reported in the literature (ε_M = 11,500 M^{-1} cm^{-1} at 25 °C) [24]. The percentage of released Doxo was calculated on the basis of the residual concentration of Doxo inside the Float-A-Lyzer® G2 system with respect to the drug concentration at time 0. The analysis was performed in triplicate. The procedure was preliminarily validated by assessing the release of free Doxo.

2.11. In vitro biological studies

2.11.1. Cell cultures

CT26 murine colorectal carcinoma and 4T1 murine mammary carcinoma cell lines were cultured using RPMI 1640 Medium supplemented with 10% Fetal Bovine Serum (FBS), 100 U/mL penicillin G sodium and 100 μg/mL streptomycin sulphate (complete medium). Cells were subcultured in 75 cm^2 culture flasks and incubated at 37 °C and 5% CO_2 atmosphere.

2.11.2. In vitro cytotoxicity

CT26 and 4T1 cell viability after incubation with Doxo or Doxo-conjugated polymeric micelles was investigated by MTT (Thiazolyl Blue Tetrazolium Bromide) assay [25]. Cells were seeded in a 96-well plate at a density of 6×10^3 cells/well (200 μL/well) and grown at 37 °C and 5% CO_2 for 24 h. Then, the medium was replaced with 100 μL of free Doxo or Doxo-conjugated polymeric micelle suspension, at 0.1–100 μM Doxo equivalent concentration range, in complete medium. Cells incubated with complete medium only were used as a control.

After 48 or 72 h of incubation, the medium was discharged and cells were gently rinsed with PBS (200 μL) and incubated with 200 μL of MTT solution in complete medium (0.5 mg/mL) for 3 h at 37 °C. Afterwards, the medium was removed and DMSO (200 μL) was added to each well to dissolve the formazan crystals. The absorbance at λ = 560 nm was measured by a Thermo Fisher Scientific MultiSkan EX plate reader (Waltham, MA, USA). Cell viability was expressed as relative percentage of living cells with respect to the untreated ones, considered as negative control ($N = 3$, $n = 17$).

2.11.3. Haemolysis

Erythrocytes (RBCs) were isolated from heparinized mouse blood by centrifugation at 500 x*g* for 5 min at 4 °C. The pellet was washed thrice with sterile saline solution (0.9% *w/v* NaCl in Milli-Q water) and resuspended in PBS, pH 7.4, to yield a 5% w/v haematocrit concentration. Afterward, volumes of 40 μL of RBC suspensions were mixed with 160 μL of $mPEG_{5kDa}$-b-$[(Doxo\text{-}hydGlu)_6$-*r*-$Leu_{10}]$ colloidal suspension in PBS, pH 7.4, or Caelyx® at equivalent Doxo concentrations in the 0–600 μM range. Samples were prepared in quadruplicate and incubated at 37 °C for 1 h and then centrifuged at 500 x*g* for 5 min. 100 μL of supernatants were plated in a 96-well plate and the released haemoglobin was quantified spectrophotometrically at 405 nm using a VICTOR X3 plate reader (PerkinElmer, Waltham, MA-USA). Absorbance of $mPEG_{5kDa}$-b-$[(Doxo\text{-}hydGlu)_6$-*r*-$Leu_{10}]$ colloidal suspensions in PBS at the tested concentrations were subtracted from each sample. The haemolytic activity of $mPEG_{5kDa}$-b-$[(Doxo\text{-}hydGlu)_6$-*r*-$Leu_{10}]$ was plotted as percentage of haemoglobin released with respect to RBC samples lysed with 1% *w/v* Triton X-100. RBCs incubated with PBS were used as negative control.

2.11.4. Confocal microscopy imaging

CT26 cells were seeded in 24-well plates containing glass dishes at a density of 5×10^4 cells/well (500 μL/well) in complete medium and allowed to grow for 24 h under culture conditions. Afterwards, the medium was discharged and replaced with 500 μL of free Doxo or micelles assembled with $mPEG_{5kDa}$-b-$[(Doxo\text{-}hydGlu)_6$-*r*-$Leu_{10}]$ at 5 μM Doxo equivalent concentration in complete medium. Cells were

incubated at 37 °C for 2 h or, after removal of the medium and cell wash with 400 μL of PBS, further incubated with complete medium for other 4 h. Afterwards, cells were gently rinsed twice with PBS (400 μL), fixed for 20 min at room temperature in the dark with 400 μL of 4% *w/v* paraformaldehyde (PFA) solution in PBS and rinsed with PBS (3 × 400 μL). Then, cells were incubated for 45 min at room temperature with 400 μL of PBS containing 5% *v*/v Rat Serum and 0.25% v/v Triton® X-100 to permeabilize the cell membrane. Afterwards, the solution was discharged, and the cells were stained for lysosomes detection. Cells were incubated with 200 μL of rat anti-mouse anti-lysosomal-associated membrane protein 1 (anti-LAMP-1) antibody solution (1:100 dilution in PBS added of 5% rat serum). After 1 h, cells were rinsed three times with PBS and incubated for 1 h with a 2 μg/mL 4′,6-diamidino-2-phenylindole (DAPI) and chicken anti-rat IgG(H + L) cross-adsorbed secondary antibody Alexa Fluor 488 conjugated (1:500 dilution) solution in PBS added of 5% fetal bovine serum (200 μL), for nuclei and lysosome staining, respectively.

Finally, the wells were gently rinsed three times with PBS and once with MilliQ water before being mounted on microscope slides using Mowiol as mounting media prepared with 10 *w/v*% of Mowiol® 4–88 and 0.1% w/v 1,4-diazabicyclo[2.2.2]octane (DABCO; Sigma-Aldrich; St Louis, MO, USA) in a 1:3.8 *v*/v glycerol/66 mM Tris-HCl buffer pH 8.5 mixture. Cells were imaged with a LSM 800 series Zeiss™ confocal laser-scanning microscope (Jena, Germany) equipped with a 63× oil immersion objective lens. Laser irradiation at 408, 488, 561 nm was used to detect DAPI for nuclei imaging (blue), anti-LAMP-antibody for lysosome imaging (green), Doxo (red), respectively. The images were then processed with ZEN 2 (blue edition) from Zeiss™ Software and elaboration was performed using ImageJ Software version 1.51j8.

2.12. In vivo studies

The animal experiments were performed according to the Belgian national regulation guidelines and in agreement with EU Directive 1010/63/EU concerning the use of animals for experimental purposes. The experiments were approved by the ethical committee for animal care of the Faculty of Medicine of the Université Catholique de Louvain (2017/UCL/MD/34). Mice had free access to water and food and the animal body weight was constantly monitored.

2.12.1. Anticancer activity on subcutaneous colorectal tumor model

CT26 cells (5×10^5 cells/mouse) were subcutaneously injected into the right flank of the mice to allow reproducible tumor volume measurements using an electronic caliper. Tumor volume was calculated according to the formula: volume = π/6 x length x width^2 [26]. Mice were randomly assigned to treatment group when the tumor reached the volume of 25 ± 2 mm^3. Treatments were administered by local intratumor injection or by tail vein intravenous injection. Five groups were set: Group 1: control group (untreated, $n = 9$); Group 2: intratumor injection of Doxo, (30 μL, $n = 7$); Group 3: intratumor injection of micelles assembled with mPEG$_{5kDa}$-b-[(Doxo-hydGlu)$_6$-*r*-Leu$_{10}$] (30 μL, $n = 6$); Group 4: intravenous injection of Doxo (150 μL, n = 7); Group 5: intravenous injection of micelles assembled with mPEG$_{5kDa}$-b-[(Doxo-hydGlu)$_6$-*r*-Leu$_{10}$] (150 μL, $n = 8$). The injected drug doses were 2.4 mg/kg and 12 mg/kg, for the intratumor and intravenous administration, respectively. The therapeutic effect was evaluated by measuring the tumor volume every other day. Body weights were assessed prior to each tumor volume measurement. The experimental end point was set when the tumor volume reached 800 mm^3 or at 20% body weight loss. When either of the last two conditions appeared, mice were sacrificed.

2.12.2. Anticancer activity on subcutaneous breast tumor model

4T1 cells (1×10^6 cells/mouse) were subcutaneously injected into the BALB/c mice right flank, and the tumor growth was monitored with the procedure described above. Mice were randomly assigned to treatment group when the tumor volume reached 26 ± 1 mm^3. Treatments were administered by local intratumor injection or by tail vein intravenous injection. Eight groups were set: Group 1: control group (untreated, $n = 9$); Group 2: intratumor injection of Doxo (30 μL, $n = 11$); Group 3: intratumor injection of micelles assembled with mPEG$_{5kDa}$-b-[(Doxo-hydGlu)$_6$-*r*-Leu$_{10}$] (30 μL, $n = 10$); Group 4: intravenous injection of Doxo (150 μL, $n = 8$); Group 5: single intravenous injection of micelles assembled with mPEG$_{5kDa}$-b-[(Doxo-hydGlu)$_6$-*r*-Leu$_{10}$] (150 μL, n = 8); Group 6: single intravenous injection of Caelyx® (150 μL, n = 8); Group 7: three intravenous injections (once per week) of micelles assembled with mPEG$_{5kDa}$-b-[(Doxo-hydGlu)$_6$-*r*-Leu$_{10}$] (150 μL, n = 8); Group 8: three intravenous injections (once per week) of Caelyx® (150 μL, $n = 7$). The dose of drug intratumorally injected was 3 mg/kg, while it was 15 mg/kg for each intravenous injection. Tumor growth was assessed by caliper measurement; body weight and tumor volume were checked every three days. The experimental endpoints were set at tumor volume of 800 mm^3, 20% body weight loss or metastasis-related side effects. When either of these conditions appeared, mice were sacrificed.

2.12.3. Toxicity studies

Six-weeks old BALB/c female mice were randomly assigned into three groups ($n = 6$) and each group received one intravenous injection of mPEG$_{5kDa}$-b-[(Doxo-hydGlu)$_6$-r-Leu$_{10}$ or Caelyx® at equivalent dose (15 mg/kg DOX) or control (PBS). Collection of blood in Sarstedt Microvette 500 tubes were performed at day 3 after injection.

Aspartate aminotransferase (AST), alanine aminotransferase (ALT), blood urea nitrogen (BUN), creatine phosphokinase (CPK), and lactate dehydrogenase (LDH) levels were assayed using a Fujifilm DRI-CHEM NX500i Analyzer (Fujifilm, Tokyo, Japan). After collection of blood, animals were sacrificed and organs (lungs, liver, heart, spleen) were collected in formol and underwent histological analysis.

Tissues from organs of mice underwent routine paraffin processing followed by sectioning at 4 μm and staining with Hematoxylin and Eosin (HE). Hearts were sectioned longitudinally to allow visualization of all four chambers and scored semi-quantitatively for severity of cardiac injury [27–30]. The histologic variables under investigations were: cytoplasmic vacuolation, infiltration by mononuclear cells, and interstitial fibrosis with myofiber disorganization/atrophy. Each criterion was scored on a 4-point scale (Table SI-1). Uncommon histologic findings (mineralization, atrial thrombosis, perivascular lymphocytes) were recorded by region as absent (0) or present (1). The scores for each anatomical region were summed to obtain a total cardiac score for each animal. For bilateral lung sections, semi-quantitative lung scoring (Table SI-1) was achieved by recording the approximate percentage per section occupied by a series of interstitial and parenchymal lesions. Scores for each change were summed to obtain a composite score. A similar approach was used to score liver and spleen pathology (Table SI-1). The pathologist was blinded as to treatment status and mouse strain.

2.13. Statistical analysis

Statistical analysis was performed using GraphPad Prism, version 7.0a (GraphPad Software, USA). All results are expressed as mean ± standard deviation (SD), except for results arising from cellular *in vitro* and *in vivo* studies which are expressed as mean ± standard error of the mean (SEM). The half maximal inhibitory concentration (IC_{50}) values were calculated using a nonlinear regression log(inhibitor) *vs* response, variable slope. Statistical significance was attained for values of $p < 0.05$ and determined using two-way ANOVA for the *in vitro* and *in vivo* studies (mouse body weight *vs* time; tumor growth *vs* time). Survival curves were compared using a Mantel-Cox (log-rank) test. Outliers were calculated using GraphPad software (significance level 0.01, two-sided) and removed from the study.

3. Results and discussion

The amphiphilic *co*-polymers [mPEG$_{5kDa}$-b-(hydGlu$_m$-*r*-Leu$_n$)]

described in this study were designed to yield self-assembling doxorubicin (Doxo) conjugates for tumor drug delivery. The co-polymers were synthetized by Ring-Opening Polymerization [31] of γ-benzyl-glutamic acid *N*-carboxyanhydride (BnOGlu-NCA) and leucine *N*-carboxyanhydride (Leu-NCA), using $mPEG_{5kDa}$-NH_2 as initiator.

Glutamic acid (Glu) was chosen as pendant group because its γ-carboxyl group can be switched to hydrazide (hydGlu) and conjugate Doxo through a pH-cleavable hydrazone bond, which intracellularly releases the drug in an acidic lysosomal microenvironment. Leucine (Leu) was included because its hydrophobic sidechain favors the self-assembly of these amphiphilic block co-polymers and enhances the stability of the resulting colloidal systems. Furthermore, Leu residues can space the Glu monomers engaged for Doxo conjugation, limiting hindrance constraints. Studies reported in the literature show, in fact, that the conjugation of Doxo to poly-aspartic acid through hydrazide bond yields only partial aspartate functionalization with the drug. This results in a heterogeneous product, with non-controlled composition and a number of unreacted pendant hydrazide groups [32] that can affect the self-assembling behavior of these polymer conjugates, the stability of resulting nanovehicles and, ultimately, the drug release. Therefore, we aimed at identifying strategies that allow for both complete derivatization of the pendant carboxylic groups of polyaminoacid-based materials, and formation of stable self-assembled delivery nanovectors. Accordingly, we designed a library of $mPEG_{5kDa}$-b-(hydGlu$_m$-*r*-Leu$_n$) diblock *co*-polymers with different Glu/Leu composition (Fig. 1).

The 5 kDa mPEG-NH_2 initiator was selected because it has been approved for systemic pharmaceutical application [33], and has already been successfully utilized to generate polyaminoacid-based self-assembling systems [34]. Indeed, PEGylation contributes to the amphiphilicity of materials including supramolecular systems and colloidal surfaces, providing a flexible, hydrated coating to the self-assembled systems, which is a requisite for "stealth" features and long circulation time in blood [35].

γ-benzyl-glutamic acid *N*-carboxyanhydride (BnOGlu-NCA) and leucine *N*-carboxyanhydride (Leu-NCA) monomers were synthesized by γ-benzyl glutamate and leucine reaction with triphosgene in the presence of α-pinene to trap HCl generated in the process (Scheme 1) [17]. Aminoacid benzyl ester protection was used to avoid possible side-reactions of γ-carboxyl group of Glu during NCA monomer synthesis and subsequent polymerization reactions. Furthermore, after polymerization the γ-benzyl ester can be straightforward converted into the corresponding γ-hydrazide moiety required for Doxo conjugation. Both NCA monomers were isolated in high purity by crystallization (BnOGlu-NCA) or precipitation (Leu-NCA).

The macroinitiator $mPEG_{5kDa}$-NH_2 was synthesized through a two-step procedure which involves the introduction at the polymer chain-end of a 1-alkene moiety, which can then be used to introduce a primary amine functionality by thiol-ene reaction [36] in the presence of cysteamine. Firstly, $mPEG_{5kDa}$-OH was converted into the $mPEG_{5kDa}$-allyl carbamate by treatment with allyl isocyanate in the presence of triethylamine. The ^{1}H NMR analysis confirmed the formation of carbamate derivative. Then, thiol-ene reaction [36] was carried out using cysteamine in the presence of DPAP as the photo-initiator that was activated at λ = 350 nm. The conversion of $mPEG_{5kDa}$-OH into $mPEG_{5kDa}$-NH_2, with a number-average molecular mass of 5.4 kDa, was confirmed by ^{1}H NMR and MALDI ToF mass spectrometry (Fig. SI-1-SI-3).

The PEG/polyaminoacid block molecular weight ratio was selected according to the literature data for analogous block *co*-polymers, where 12 kDa mPEG was used as initiator of a 37 aspartic acid monomer block [32]. In order to investigate the effect of the co-polymer composition on the physicochemical properties of these materials and in turn the biopharmaceutical performance of the drug conjugates, four $mPEG_{5kDa}$-b-(hydGlu$_m$-*r*-Leu$_n$) were produced by using 1:16:0, 1:8:8, 1:6:10, 1:4:12 mPEG/BnOGlu/Leu ratio ratios (Table 1, Fig. SI-4-SI-9).

The content of BnOGlu and Leu in the polymers was estimated by ^{1}H NMR by comparing the integral of the signal of terminal -OCH_3 of mPEG at 3.3–3.4 ppm with those of benzylic -OCH_2- at 5.0–5.2 ppm of BnOGlu, and of the -CH_3 groups at 0.6–1.0 ppm of Leu (Fig. SI-10-SI-13). SEC analysis showed that all polymers had low molecular weight dispersity. The observed $M_{n,SEC}$ values were slightly higher than the ones estimated by ^{1}H NMR, which can be ascribed to the difference in hydrodynamic volume between the $mPEG_{5kDa}$-polyaminoacid materials synthesized in this study and the PMMA narrow standards utilized to calibrate the SEC.

The pendant γ-benzyl ester functionalities were converted into hydrazide moieties by treatment with hydrazine. ^{1}H NMR analysis of the purified *co*-polymers (Fig. SI-14-SI-17) showed complete removal of the benzyl ester protecting group. A modified Snyder's assay [19] showed that the number of γ-hydrazide groups per polymer chain was in agreement with the theoretically expected. SEC analysis confirmed that all final $mPEG_{5kDa}$-b-(hydGlu$_m$-*r*-Leu$_n$) *co*-polymers retained low molecular dispersity.

Doxo conjugation to the hydrazide pendant groups of the *co*-polymer was estimated by UV–Vis at λ = 488 nm in relation of the $mPEG_{5kDa}$ concentration assessed by iodine assay. The conjugation efficiency (number of Doxo derivatized hydrazide/total hydrazide) was found to be inversely correlated to the hydGlu:Leu ratio being 44, 70, 88, and 100% for $mPEG_{5kDa}$-hydGlu$_{16}$, $mPEG_{5kDa}$-b-(hydGlu$_8$-*r*-Leu$_8$), $mPEG_{5kDa}$-b-(hydGlu$_6$-*r*-Leu$_{10}$), and $mPEG_{5kDa}$-b-(hydGlu$_4$-*r*-Leu$_{12}$), respectively. This result is in good agreement with our initial hypothesis represented in Fig. 1, which postulated that hydrazide functionalities of the γ-hydGlu monomers must be sufficiently spaced along the polymer chain to minimize steric hindrance provided by grafted drug molecules.

3.1. Characterization of polymeric micelles

The critical micelle concentration (CMC) of drug-free $mPEG_{5kDa}$-b-(hydGlu$_m$-*r*-Leu$_n$) *co*-polymers was assessed using pyrene as a fluorescent probe. The CMC was calculated by elaboration of results of Fig. 2A-D that reports the plots of the emission intensity ratio of the third (I_3) and first (I_1) spectrum signals of the pyrene spectrum *vs* the logarithmic polymer concentration [37].

In agreement with results reported by Vega et al. for PEG-polyGlu based materials [38], $mPEG_{5kDa}$-hydGlu$_{16}$ did not self-assemble under the experimental conditions used for the CMC assay (CMC > 300 μM). On the contrary, $mPEG_{5kDa}$-b-(hydGlu$_8$-*r*-Leu$_8$), $mPEG_{5kDa}$-b-(hydGlu$_6$-*r*-Leu$_{10}$) and $mPEG_{5kDa}$-b-(hydGlu$_4$-*r*-Leu$_{12}$) were found to assemble with CMC of 92.2 ± 13.1 μM, 78.5 ± 8.6 μM, and 17.8 ± 13.1 μM,

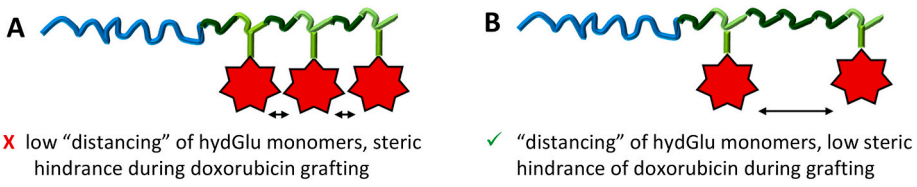

Fig. 1. Schematic representation of $mPEG_{5kDa}$-b-[(Doxo-hydGlu)$_m$-*r*-Leu$_n$] with high (A) and low (B) ratio of hydGlu monomers with respect to Leu. Light green sections: hydGlu monomer; dark green sections: Leu monomer; light blue chain: PEG; red stars: Doxo. (For interpretation of the references to colour in this figure legend, the reader is referred to the web version of this article.)

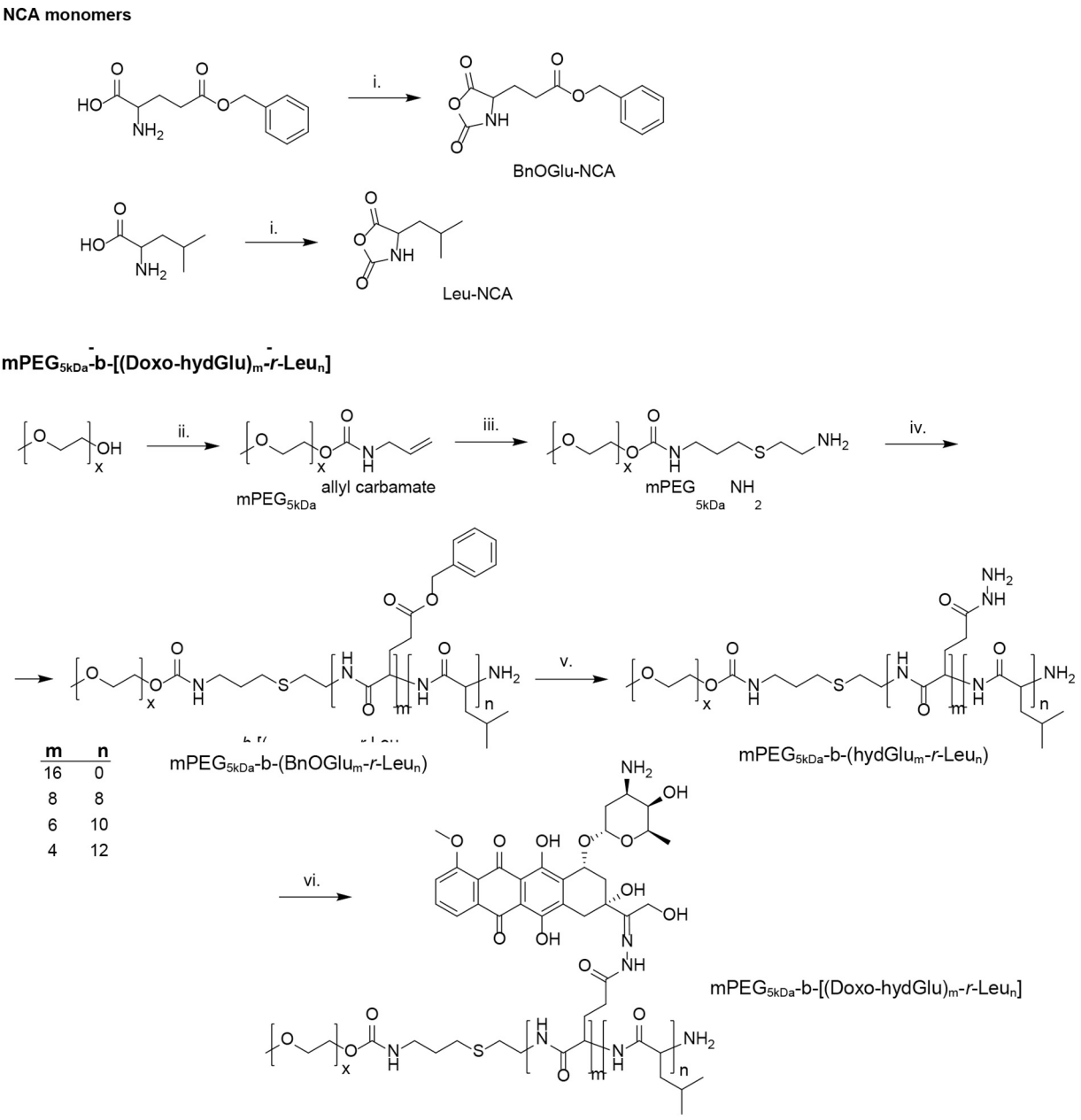

Scheme 1. Synthesis of $mPEG_{5kDa}$-b-[(Doxo-hydGlu)$_m$-*r*-Leu$_n$]. i. triphosgene, α-pinene, THF, 56 °C, 90 min; ii. allyl isocyanate, Et_3N, $CHCl_3$, room temperature, 18 h; iii. Cysteamine hydrochloride, DPAP, MeOH, irradiation at λ = 350 nm, 3 h; iv. BnOGlu-NCA, Leu-NCA, DMF, room temperature, 7 days; v. hydrazine hydrate, DMF, 40 °C, 48 h; vi. Doxo hydrochloride, TFA 0.2% (*v*/v), DMSO, 3 days.

respectively. These results show that, as expected, the increase of Leu/Glu molar ratio favors the *co*-polymer assembling, which is ascribable to the hydrophobic isobutyl side moiety (hydrophobic constant π = 1.64. [39]), while in the case of $mPEG_{5kDa}$-$hydGlu_{16}$, that does not contain hydrophobic moieties, assembling does not occur.

Due to fluorescence interferences between Doxo and pyrene, a novel analytical procedure was set-up to calculate the CMC of Doxo conjugated $mPEG_{5kDa}$-b-(hydGlu$_m$-*r*-Leu$_n$) *co*-polymers, which exploits the Doxo emission intensities at 555 nm. This analytical approach relies on the quenching of the Doxo fluorescence when drug molecules are in close proximity such as in the core of micelles [40,41].

Fig. 2E-G reports the plots of emission intensities of Doxo at 555 nm *vs* the concentration of the $mPEG_{5kDa}$-b-[(Doxo-hydGlu)$_m$-*r*-Leu$_n$] *co*-polymers that were used to calculate the CMC. The increase of drug-polymer concentration resulted in a linear increase of the spectrophotometric absorbance of Doxo at λ = 488 nm (Fig. SI-18) while the fluorescence emission intensity at λ = 555 nm initially increased and then decreased as consequence of the fluorophore self-quenching when the polymers self-assemble (Fig. SI-19).

In this work, we observed that the high leucine content combined with the presence of four Doxo molecules in $mPEG_{5kDa}$-b-[(Doxo-hydGlu)$_4$-*r*-Leu$_{12}$] resulted in conjugate precipitation into large aggregates. Therefore, this Doxo-conjugate block co-polymer could not be characterized and further investigated *in vitro* and *in vivo*.

The different fluorescence profiles reported in Fig. 2 E-G reflect the co-polymer composition. Indeed, as the Leu content increases a lower Doxo packing can be achieved that reflects on lower quenching rate as the micelles assemble. Therefore, the CMC values were calculated at the intercept of the regression lines of increasing and decreasing fluorescence. The CMC for $mPEG_{5kDa}$-(Doxo-hydGlu)$_{16}$, $mPEG_{5kDa}$-b-[(Doxo-hydGlu)$_8$-*r*-Leu$_8$] and $mPEG_{5kDa}$-b-[(Doxo-hydGlu)$_6$-*r*-Leu$_{10}$] were 6.7 ± 0.9 μM, 4.9 ± 0.2 μM, and 4.6 ± 0.2 μM, respectively. The CMC of the

Table 1
Composition and molecular weight features of co-polymers synthesized in this work.

Polymers[a]	Glu: Leu[a]	$M_{n,\ NMR}$ (kDa)[a]	$M_{n,\ SEC}$[b] (kDa)	Đ[b]
$mPEG_{5kDa}$-$BnOGlu_{16}$	16:0	9.3	12.2	1.07
$mPEG_{5kDa}$-b-($BnOGlu_8$-*r*-Leu_8)	8:8	8.2	10.5	1.11
$mPEG_{5kDa}$-b-($BnOGlu_6$-*r*-Leu_{10})	6:10	8.0	10.4	1.09
$mPEG_{5kDa}$-b-($BnOGlu_4$-*r*-Leu_{12})	4:12	7.8	9.9	1.08
$mPEG_{5kDa}$-$hydGlu_{16}$	16:0	8.1	12.2	1.03
$mPEG_{5kDa}$-b-($hydGlu_8$-*r*-Leu_8)	8:8	7.6	8.9	1.25
$mPEG_{5kDa}$-b-($hydGlu_6$-*r*-Leu_{10})	6:10	7.5	8.8	1.15
$mPEG_{5kDa}$-b-($hydGlu_4$-*r*-Leu_{12})	4:12	7.4	9.8	1.20

[a] Co-polymers composition was estimated by ^1H NMR in $CDCl_3$.
[b] Determined by SEC using DMF + 0.1% LiBr as the mobile phase, in a system calibrated with PMMA standards.

$mPEG_{5kDa}$-b-[(Doxo-Glu)$_m$-*r*-Leu$_n$] was also assessed by light scattering using a detection system equipped with fluorescent filter for Doxo fluorescence removal, which provided CMC values in agreement with those obtained by fluorescence quenching analysis (Fig. SI-20). Interestingly, the CMC values of copolymers containing Doxo are about 20-fold lower than the ones obtained with the Doxo-free counterparts indicating that Doxo plays a relevant role in copolymer association and micelle packing. To note that the low CMC of $mPEG_{5kDa}$-b-[(Doxo-Glu)$_m$-*r*-Leu$_n$] is a requisite for therapeutic applications of these delivery systems. Indeed, low CMC prevents the dissociation of the nanocarrier upon dilution in the blood.

The size of the colloidal systems is relevant in dictating the fate of a nanocarrier after injection in the bloodstream. Indeed, the diameter of the nanosized therapeutics suitable for *in vivo* application should lay in the range from 5 to 200 nm, which minimizes the renal clearance through the glomerular capillaries occurring for colloids with size below 5 nm, and the RES removal for colloids with size above 200 nm [42].

Table 2 reports the size, polydispersity index and charge of the assemblies obtained with drug-free and Doxo-conjugated *co*-polymers.

$mPEG_{5kDa}$-b-($hydGlu_8$-*r*-Leu_8) and $mPEG_{5kDa}$-b-($hydGlu_6$-*r*-Leu_{10}) micelles had similar size, while the $mPEG_{5kDa}$-b-($hydGlu_4$-r-Leu_{12}) nanoparticles showed slightly smaller diameter with no statistically significant differences although a decreasing size trend was observed with the increase of Leu content, suggesting that Leu may have a little influence on the size of the micelles.

The results reported in Table 2 show that the $mPEG_{5kDa}$-(Doxo-$hydGlu)_{16}$, $mPEG_{5kDa}$-b-[(Doxo-$hydGlu)_8$-*r*-Leu_8] and $mPEG_{5kDa}$-b-

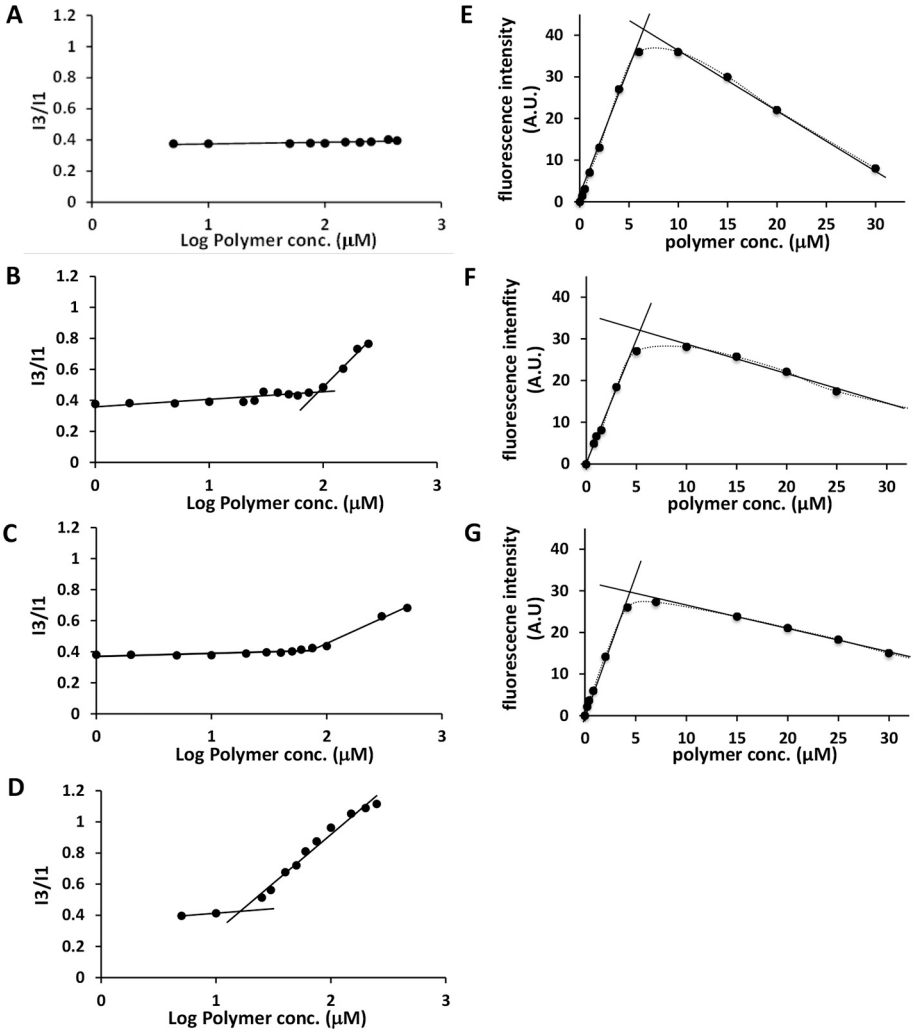

Fig. 2. Self-assembly behavior of the polymer library. I_3/I_1 spectrum signal ratio of pyrene *vs* logarithmic concentration of (A) $mPEG_{5kDa}$-$hydGlu_{16}$, (B) $mPEG_{5kDa}$-b-($hydGlu_8$-*r*-Leu_8), (C) $mPEG_{5kDa}$-b-($hydGlu_6$-*r*-Leu_{10}), and (D) $mPEG_{5kDa}$-b-($hydGlu_4$-*r*-Leu_{12}). Fluorescence intensity at 555 nm (arbitrary units: A.U.) of (E) $mPEG_{5kDa}$-(Doxo-$hydGlu)_{16}$, (F) $mPEG_{5kDa}$-b-[(Doxo-$hydGlu)_8$-*r*-Leu_8], (G) $mPEG_{5kDa}$-b-[(Doxo-$hydGlu)_6$-*r*-Leu_{10}] *vs* conjugate concentration.

Table 2
Volume weighted hydrodynamic diameter (d_H), PDI and zeta potential (ZP) obtained by DLS analysis; diameter assessed by TEM analysis (d_{TEM}) of $mPEG_{5kDa}$-b-($hydGlu_m$-r-Leu_n) and $mPEG_{5kDa}$-b-[$(Doxo\text{-}hydGlu)_m$-r-Leu_n] assemblies. (ND: non-detectable; NA non-assessable).

	d_H (nm)	PDI	d_{TEM} (nm)	ZP (mV)
$mPEG_{5kDa}$-$hydGlu_{16}$	ND	ND	ND	ND
$mPEG_{5kDa}$-b-($hydGlu_8$-*r*-Leu_8)	51.0 ± 4.2	0.37 ± 0.07	47.9 ± 3.9	0.46 ± 0.17
$mPEG_{5kDa}$-b-($hydGlu_6$-*r*-Leu_{10})	50.2 ± 4.1	0.39 ± 0.05	45.5 ± 4.3	0.23 ± 0.02
$mPEG_{5kDa}$-b-($hydGlu_4$-*r*-Leu_{12})	39.2 ± 5.6	0.30 ± 0.04	32.3 ± 3.4	0.03 ± 0.32
$mPEG_{5kDa}$-$(Doxo\text{-}hydGlu)_{16}$	41.6 ± 4.9	0.34 ± 0.06	38.4 ± 4.5	2.31 ± 0.25
$mPEG_{5kDa}$-b-[$(Doxo\text{-}hydGlu)_8$-*r*-Leu_8]	33.3 ± 5.3	0.37 ± 0.05	26.5 ± 3.0	3.36 ± 0.25
$mPEG_{5kDa}$-b-[$(Doxo\text{-}hydGlu)_6$-*r*-Leu_{10}]	29.2 ± 1.1	0.36 ± 0.07	23.8 ± 3.0	3.61 ± 0.28
$mPEG_{5kDa}$-b-[$(Doxo\text{-}hydGlu)_4$-*r*-Leu_{12}]	NA	NA	NA	NA

[$(Doxo\text{-}hydGlu)_6$-*r*-Leu_{10}] assemble into colloidal systems with smaller hydrodynamic diameter with respect to the drug-free counterparts. The smaller size of Doxo-loaded micelles compared to the Doxo-free counterparts can be ascribed to structural arrangements. The role played by Doxo in the formation of micelles is also supported by the evidence that $mPEG_{5kDa}$-$(Doxo\text{-}hydGlu)_{16}$ can self-assemble into nanoparticles while $mPEG_{5kDa}$-b-[$(Doxo\text{-}hydGlu)_4$-*r*-Leu_{12}] could not be analyzed by DLS due to formation of large aggregates that underwent precipitation. To note that, similarly to the Doxo free conjugates, the Doxo containing counterparts showed a micelle size decrease trend with the increase of Leu content, although no statistical significance was calculated along the copolymer series.

The TEM images of Doxo conjugates reported in Fig. 3 show that all block *co*-polymers containing Leu formed similar homogeneous nanostructures with round shaped morphology typical of micelles formed by block co-polymer where hydrophilic block is longer than the hydrophobic portion of an amphiphilic co-polymer [43]. The size was in agreement with the results obtained by DLS analyses (Fig. 3, Fig. SI-22, Table SI-2). The non-spherical shape of the micelles observed by TEM may explain the relatively high PDI obtained by DLS analysis. However, it should be noted that high PDI have been already reported in the literature in the case of self-assembling amphiphilic co-polymers [44].

Importantly, micelles were found to be fairly stable even in the presence of proteins over 72 h of incubation at 37 °C either at pH 7.4 or 5.5. Indeed, the DLS results (Fig. SI-23) showed that the micelles did not undergo aggregation, even though the standard deviation was higher than that obtained in buffer, which is ascribable to detection interferences due to the presence of proteins.

Altogether, the TEM and DLS results confirmed that the micellar nanosystems obtained with the new block co-polymers loaded with Doxo possess a suitable size for the passive tumor accumulation through the EPR effect [45–47].

The zeta potential analysis revealed that $mPEG_{5kDa}$-b-($hydGlu_m$-*r*-Leu_n) micelles are close to neutrality, which is in agreement with the mostly non-protonated state of the hydrazide groups at pH 7.4 being the pK_a typically in the range of 4–5 [48]. The $mPEG_{5kDa}$-b-[$(Doxo\text{-}hydGlu)_m$-*r*-Leu_n] micelles possess a slightly positive zeta potential, which can be ascribed to exposure of the amino group of the gluconic moiety of few Doxo units.

3.2. Release studies

Doxo release from the micelles was investigated at pH 7.4 and 5.5, which correspond to the bloodstream and lysosomal pH, respectively.

The release profiles reported in Fig. 4 show that the drug loaded formulations {$mPEG_{5kDa}$-$(Doxo\text{-}hydGlu)_{16}$, $mPEG_{5kDa}$-b-[$(Doxo\text{-}hydGlu)_8$-*r*-Leu_8], and $mPEG_{5kDa}$-b-[$(Doxo\text{-}hydGlu)_6$-*r*-Leu_{10}]} possess similar release profile at the two pH tested, and the drug release is remarkably faster under acid conditions. The formulations displayed

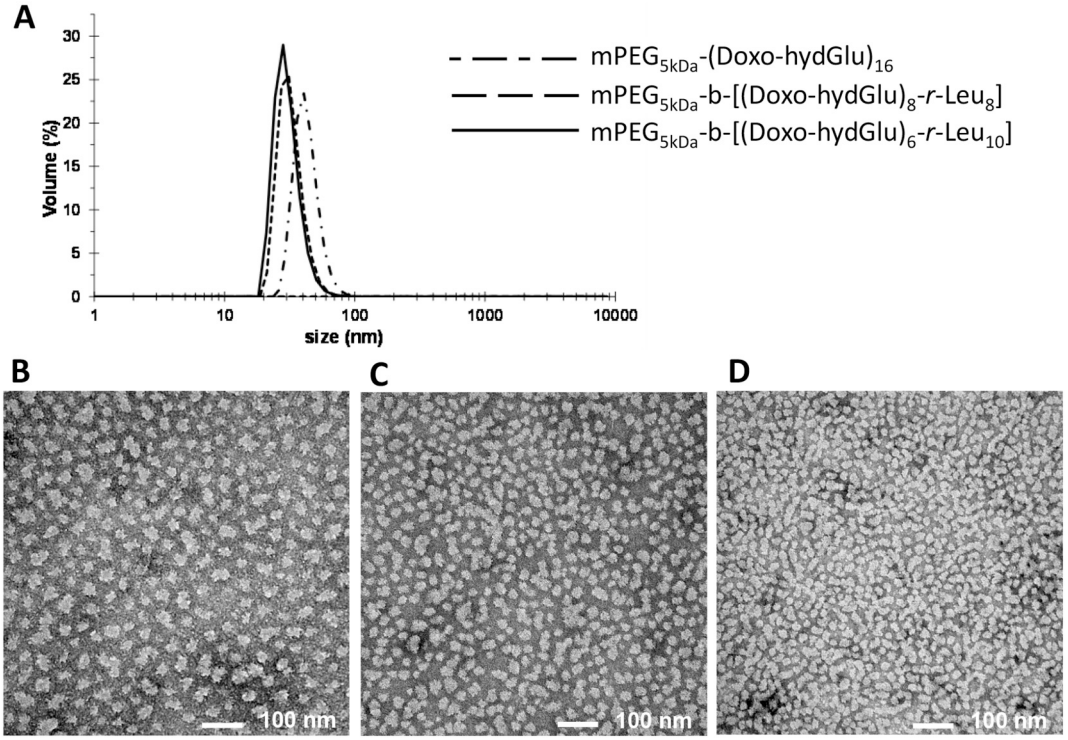

Fig. 3. Size profiles by DLS (A) and TEM images of $mPEG_{5kDa}$-$(Doxo\text{-}hydGlu)_{16}$ (B), $mPEG_{5kDa}$-b-[$(Doxo\text{-}hydGlu)_8$-r-Leu_8] (C), and $mPEG_{5kDa}$-b-[$(Doxo\text{-}hydGlu)_6$-r-Leu_{10}] (D). The TEM images underwent ImageJ analysis and histograms of the particle size distributions have been reported in Fig. SI-21.

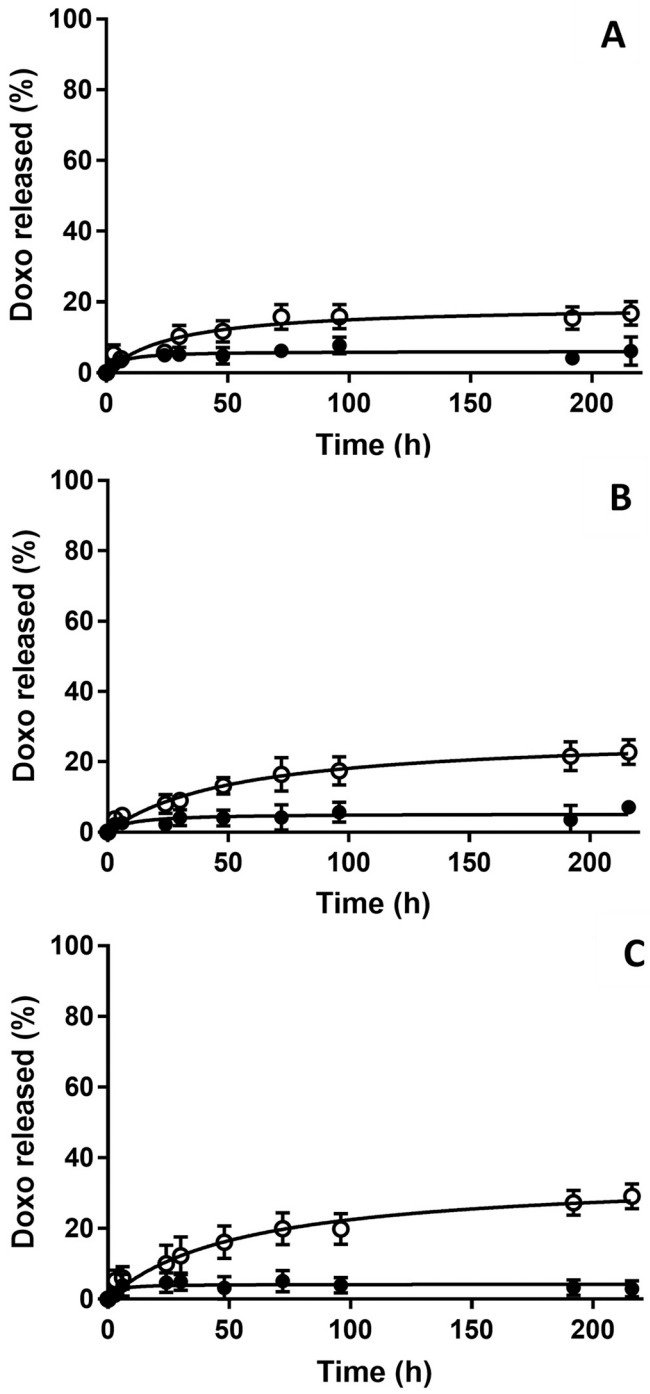

Fig. 4. Doxo release profile from (A) $mPEG_{5kDa}$-(Doxo-hydGlu)$_{16}$, (B) $mPEG_{5kDa}$-b-[(Doxo-hydGlu)$_8$-*r*-Leu$_8$], (C) $mPEG_{5kDa}$-b-[(Dox-hydGlu)$_6$-*r*-Leu$_{10}$], at pH 7.4 (●) and pH 5.5 (○).

high stability at pH 7.4 with negligible drug release over 9 days, which is crucial in preventing undesired drug release in the bloodstream (pH 7.4) upon administration, thus reducing drug-related systemic toxicity ascribable to off-target release and disposition [5,49].

At pH 5.5, Doxo was slowly released to yield 17, 23 and 29% released drug in 9 days from $mPEG_{5kDa}$-(Doxo-hydGlu)$_{16}$, $mPEG_{5kDa}$-b-[(Doxo-hydGlu)$_8$-*r*-Leu$_8$] and $mPEG_{5kDa}$-b-[(Doxo-hydGlu)$_6$-*r*-Leu$_{10}$], respectively. In general, the release rate through the hydrazone cleavage was much slower than that expected according to our experience with polymer bioconjugates and studies reported in the literature [50]. However, it should be noticed that the hydrolysis of chemical bonds is strongly affected by the microenvironment that is influenced by the structure of the supramolecular system. Interestingly, the profiles reported in Fig. 4 show that the Doxo release rate increases with the Leu content in the conjugate. In particular, statistically significant differences were found after 100 h of drug release between $mPEG_{5kDa}$-(Doxo-hydGlu)$_{16}$ and $mPEG_{5kDa}$-b-[(Dox-hydGlu)$_6$-*r*-Leu$_{10}$]. Indeed, considering that the drug is conjugated to the backbone in the same way in all copolymers, it seems reasonable to think that differences in drug release are due to the different access of water in the micelle core as reported above which suggests that Leu and the resulting different intermolecular interactions within the micelle core play a role in the drug release profile.

Finally, despite the slow drug release observed in buffer, it is worth mentioning that the drug release rate in the acid intracellular compartments may be facilitated by the contribution of lysosomal enzymatic fragmentation as reported in the literature with other Doxo conjugated poly(L-glutamic acid) based therapeutics [51].

3.3. Cell viability studies

As Doxo has demonstrated its therapeutic efficacy against several solid tumors, $mPEG_{5kDa}$-(Doxo-hydGlu)$_{16}$, $mPEG_{5kDa}$-b-[(Doxo-hydGlu)$_8$-*r*-Leu$_8$], and $mPEG_{5kDa}$-b-[(Doxo-hydGlu)$_6$-*r*-Leu$_{10}$] micelles were tested on two tumor cell lines, murine colorectal carcinoma CT26 [52,53] and murine mammary carcinoma 4T1 [54]. Their anticancer effect was investigated by MTT assay following cells treatment with equivalent Doxo concentrations in the range of 0.1–100 μM for 48 or 72 h. A preliminary study was undertaken to evaluate the biocompatibility of the drug free block *co*-polymers at concentrations corresponding to the maximum equivalent concentrations used with the Doxo loaded bioconjugates, namely 13 μM for $mPEG_{5kDa}$-hydGlu$_{16}$, $mPEG_{5kDa}$-b-(hydGlu$_8$-*r*-Leu$_8$), and 18 μM for $mPEG_{5kDa}$-b-(hydGlu$_6$-*r*-Leu$_{10}$) for 72 h. In all cases, the CT26 and 4 T1 cell viability resulted to be above 80% (Fig. SI-24) indicating that the co-polymers have high biocompatibility, which is a requisite for therapeutic applications.

Fig. 5A reports the cell viability profiles of both CT26 and 4 T1 cell lines incubated with the drug-conjugates. Pharmacologically active Doxo is released after the hydrazone bond cleavage, which is a requisite for its localization into the nucleus of cancer cells and DNA intercalation [11].

In the case of CT26 cells, the IC_{50} obtained with the two bioconjugates containing Leu were higher than free Doxo and decreased with the incubation time. The $mPEG_{5kDa}$-(Doxo-hydGlu)$_{16}$ had similar IC_{50} after 48 h and 72 h incubation. After 72 h cell incubation all bioconjugates showed similar IC_{50} (Fig. 5-B1).

The cytotoxicity towards 4T1 cancer cells was similar for all bioconjugates and at both tested incubation times (Fig. 5-B2). The similar IC_{50} at 48 and 72 h might be ascribed to the rapid proliferation and aggressiveness of these cells that may develop drug resistance. The lower IC50 observed with 4T1 cells with respect to CT26 may be due to several factors among which cell line sensitivity to the drug, rate of bioconjugate access to the cytosolic compartment and drug availability resulting from trafficking pathways and intracellular release rate.

The cell viability profiles reported in Fig. 5-A and the IC50 data reported in Fig. 5-B show that under the experimental conditions the $mPEG_{5kDa}$-b-[(Doxo-hydGlu)$_m$-*r*-Leu$_n$] bioconjugates have biological activity comparable to Doxo, which makes these systems very promising for therapeutic applications. Indeed, usually Doxo bioconjugates possess significantly lower cytotoxicity compared to the free drug [55,56], which implies the use of high drug doses.

$mPEG_{5kDa}$-b-[(Doxo-hydGlu)$_6$-*r*-Leu$_{10}$] showed the lowest IC_{50} value in both cell lines, which can be ascribed to better cell uptake and/or to the more efficient Doxo release reported in Fig. 4.

$mPEG_{5kDa}$-b-[(Doxo-hydGlu)$_6$-*r*-Leu$_{10}$] was the *co*-polymer with highest performance in terms of derivatization efficiency of the hydGlu monomers with Doxo, drug release and biological activity *in vitro*.

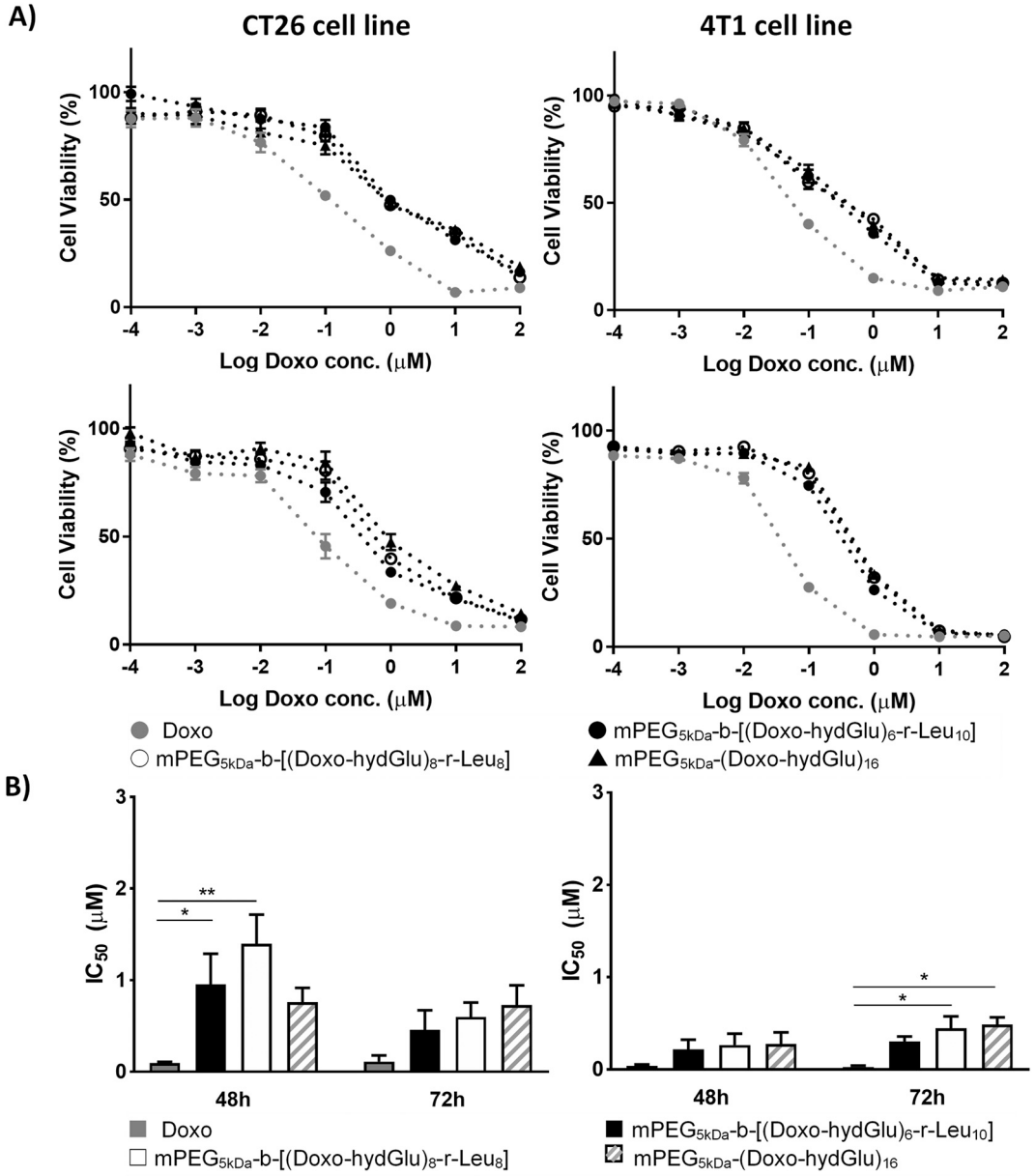

Fig. 5. A. Viability profiles of CT26 cells (left) and 4T1 cell line (right) after 48 (top panels) and 72 h (bottom panels) incubation with Doxo, $mPEG_{5kDa}$-(Doxo-hydGlu)$_{16}$, $mPEG_{5kDa}$-b-[(Doxo-hydGlu)$_8$-*r*-Leu$_8$], $mPEG_{5kDa}$-b-[(Doxo-hydGlu)$_6$-*r*-Leu$_{10}$], at drug equivalent concentration; B. IC_{50} of Doxo and micellar formulations referred as drug concentration (mean ± SEM, $N = 3$, $n = 17$) $^{***}p < 0.001$, $^{**}p < 0.01$ $^{*}p < 0.05$.

Accordingly, this bioconjugate was selected for the further *in vitro* and *in vivo* investigations.

3.4. Confocal analyses

The intracellular fate of free Doxo and $mPEG_{5kDa}$-b-[(Doxo-hydGlu)$_6$-*r*-Leu$_{10}$] in the CT26 cells was assessed by immunofluorescence confocal microscopy. The co-localization of free or conjugated Doxo (red fluorescence) within lysosomes (green fluorescence) was investigated by labeling lysosomes with primary antibody against Lysosomal-Associated Membrane Protein-1 (LAMP-1). Fig. 6 shows representative images of cells incubated with free Doxo or $mPEG_{5kDa}$-b-[(Doxo-hydGlu)$_6$-*r*-Leu$_{10}$] and for 2 h or for 2 h plus 4 h incubation with fresh complete medium.

Upon 2 h cell incubation with free Doxo, the drug fluorescence was mostly associated to the nuclei, while $mPEG_{5kDa}$-b-[(Doxo-hydGlu)$_6$-*r*-Leu$_{10}$] was mostly disposed in the lysosomal compartment (yellow spots resulting from the overlapping of micelles red spots co-localized with the lysosome green staining) or in the cytosol. This confirmed the intracellular delivery of the drug by the nanocarrier and its trafficking through the lysosomal compartment where the presence of the acidic environment can trigger the cleavage of the pH sensible hydrazone bond [57], resulting in Doxo release. $mPEG_{5kDa}$-b-[(Doxo-hydGlu)$_6$-*r*-Leu$_{10}$] persisted into lysosomes over 4 h cell incubation resulting in the released Doxo disposition in the nuclei. It is worth noting that at this time point the fluorescence in the nuclei of cells incubated with free Doxo was negligible indicating that the drug diffuses from the nucleus during incubation with medium.

3.5. In vivo studies

Based on the *in vitro* results, the anticancer activity of $mPEG_{5kDa}$-b-[(Doxo-hydGlu)$_6$-*r*-Leu$_{10}$] was tested on CT26 and 4T1 subcutaneous syngeneic tumor models [58] following intratumor (IT) and intravenous

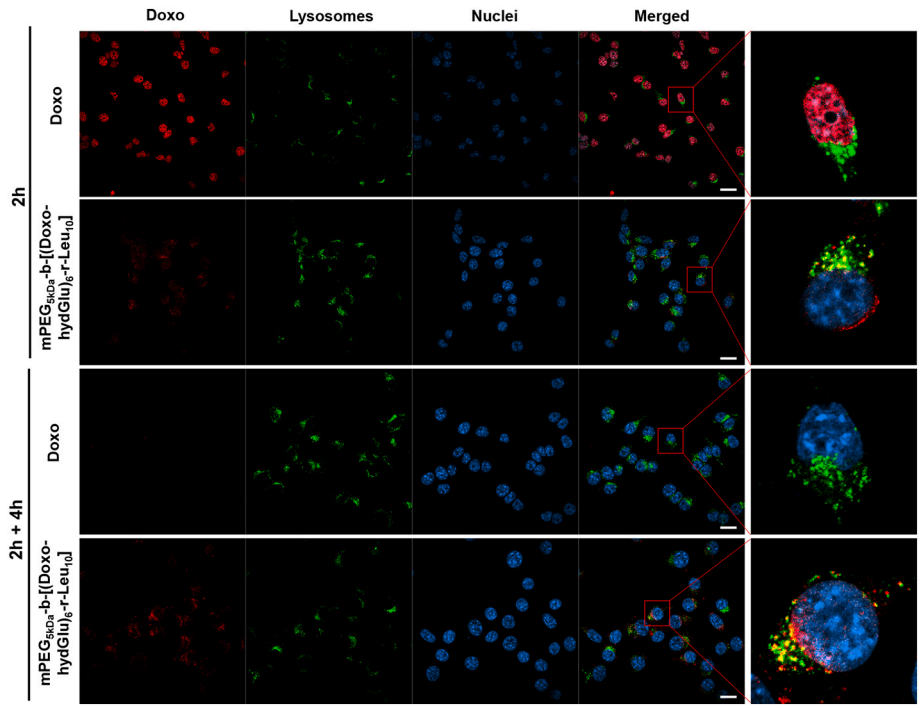

Fig. 6. Confocal microscopy images of CT26 cell incubated with: Doxo or $mPEG_{5kDa}$-b-[(Doxo-hydGlu)$_6$-*r*-Leu_{10}] for 2 h; and with Doxo or $mPEG_{5kDa}$-b-[(Doxo-hydGlu)$_6$-*r*-Leu_{10}] for 2 h followed by 4 h incubation with fresh medium. Scale bar: 20 μm.

(IV) administrations. The Doxo dose was selected according to the studies reported by Bae et al. [40] and Lv et al. [59] showing that polyaminoacidic based micellar systems display anticancer activity in mice with doses in the 10–20 mg/kg range. As the Doxo-loaded PEGylated liposomal trademark formulation Caelyx® is a nanomedicine used for breast cancer treatment, this formulation was also used as reference in our 4T1 *in vivo* studies.

A preliminary study was carried out to assess the *in vivo* toxicity of $mPEG_{5kDa}$-b-[(Doxo-hydGlu)$_6$-*r*-Leu_{10}] by intravenous administration to healthy mice of 12 mg/kg Doxo equivalent bioconjugate dose and monitoring the animal body weight and wellbeing for 14 days. No weight loss, distress or behavior changes were observed during this time, confirming the good tolerability of the bioconjugates at the selected dose (Data not shown). In the first antitumor study, free Doxo or Doxo equivalent dose of $mPEG_{5kDa}$-b-[(Doxo-hydGlu)$_6$-*r*-Leu_{10}] was administered either intratumorally or intravenously to CT26 tumor bearing mice at 2.4 mg/kg and 12 mg/kg, respectively. The intratumor administration allows for achieving higher drug dose at the tumor site while reducing the risk of side effects compared to the systemic route [60].

The intratumoral injection of mice did not induce weight loss in the week following the treatment (Fig. 7A). The intravenous administration of $mPEG_{5kDa}$-b-[(Doxo-hydGlu)$_6$-*r*-Leu_{10}] did not impact the mouse weight curve while free Doxo induced weight loss in most of the animals starting from the first few days following treatment (Fig. 7B).

$mPEG_{5kDa}$-b-[(Doxo-hydGlu)$_6$-*r*-Leu_{10}] treated mice survived longer than the untreated and free Doxo treated groups, showing a higher median survival time of 30 days and 23 days after intratumoral and intravenous administration, respectively.

Fig. 7B and E show a significant tumor growth delay after intratumor and intravenous injections of the bioconjugate with respect to the untreated group starting one week following treatment (day 15) refer to supporting information for statistical comparison between different groups, proving the therapeutic efficacy of the bioconjugate. However, no significant difference in tumor growth was observed compared to Doxo (except between day 19 and 23). $mPEG_{5kDa}$-b-[(Doxo-hydGlu)$_6$-*r*-Leu_{10}] treated mice survived longer than the untreated and free Doxo treated groups, showing a higher median survival time of 30 days and 23 days after intratumoral and intravenous administration, respectively.

The therapeutic activity of the polymeric nanocarrier was also investigated *in vivo* with 4T1-bearing mice. The animals were randomly divided into groups and treated either locally with intratumor injections of 3 mg/kg Doxo equivalent dose, or intravenously with single or multiple injections of 15 mg/kg Doxo equivalent dose (three administrations, once per week).

Fig. 8B shows that after intratumor administration, the Kaplan-Meier survival curves of Doxo and $mPEG_{5kDa}$-b-[(Doxo-hydGlu)$_6$-*r*-Leu_{10}] present similar median survival, which is higher compared to the untreated group (30 and 31 days for the Doxo and $mPEG_{5kDa}$-b-[(Doxo-hydGlu)$_6$-*r*-Leu_{10}] treated groups *vs* 27 days for the control group). Spontaneous metastases spreading from the primary tumor were observed in all the groups, which can be ascribed to the highly tumorigenic and invasive behavior of 4T1 tumor model [61]. This prompted the sacrifice of the mice for metastasis-related side effects and not for the tumor size.

Fig. 8A shows that after intratumor administration, a slight decrease of body weight was noticed for treated groups {Doxo and $mPEG_{5kDa}$-b-[(Doxo-hydGlu)$_6$-*r*-Leu_{10}]} starting from day 18. Similar body weight loss was observed for untreated mice suggesting that this was due to the metastasis onset, rather than to the toxicity of the treatment. The presence of metastasis was confirmed by autopsies, demonstrating that lungs and spleen were the organs mainly colonized by metastatic cells. Based on the tumor volume values before metastasis onset and until the moment of sacrifice, a significant difference between Doxo treated group and $mPEG_{5kDa}$-b-[(Doxo-hydGlu)$_6$-*r*-Leu_{10}] treated mice was detected (Fig. 8B; refer to supporting information for statistical comparison between different groups).

The intravenous administration to mice bearing 4T1 subcutaneous tumors was performed by single injection and weekly multiple administrations. This treatment schedule was planned on the basis of the fast tumor growth rate observed during previous studies. Free Doxo and Caelyx®, a trademark Doxo liposomal formulation approved for the treatment of several cancers including breast, ovarian and multiple myeloma [62,63], were administered as references. The high toxicity of free Doxo observed after a single injection to the CT26 cancer bearing

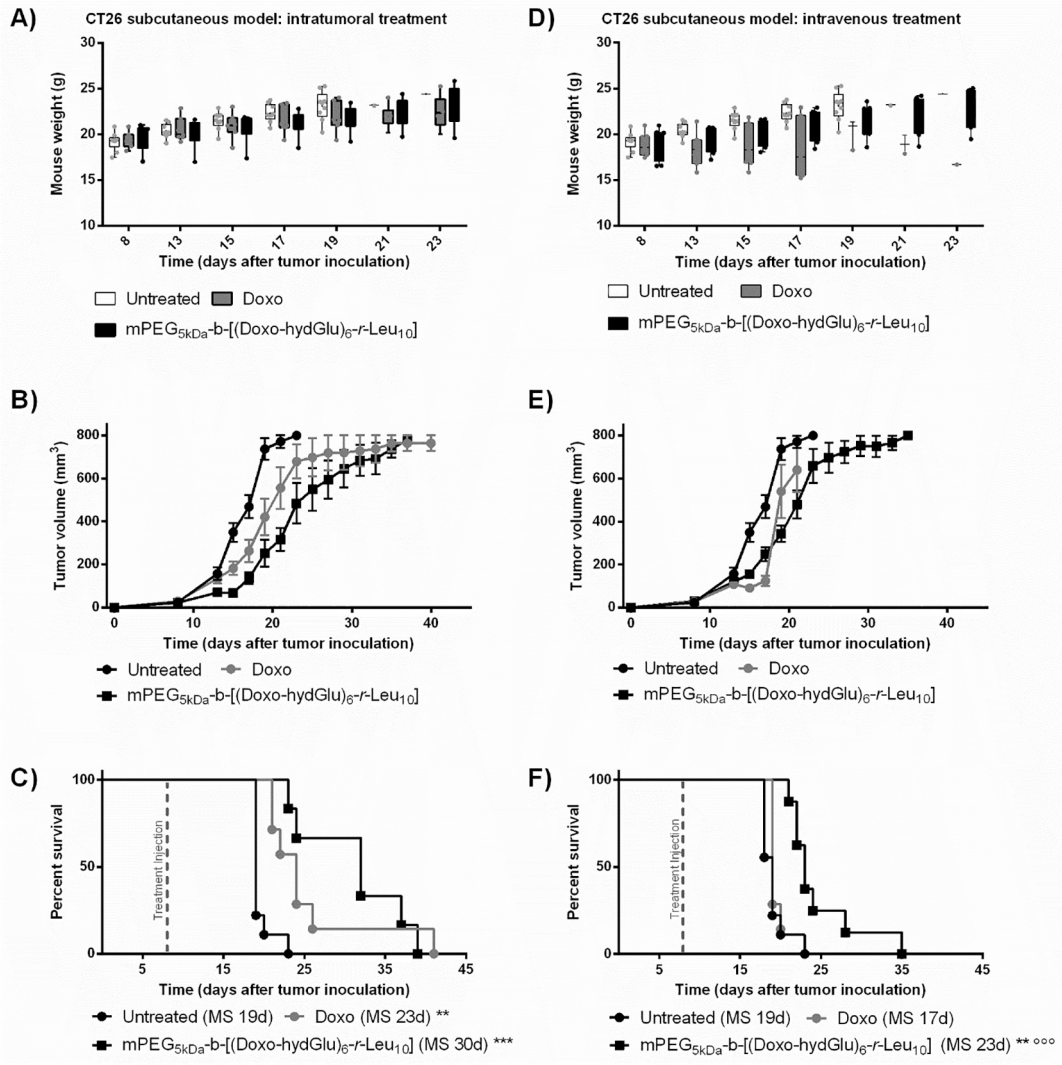

Fig. 7. *In vivo* antitumor efficacy of $mPEG_{5kDa}$-b-[(Doxo-hydGlu)$_6$-*r*-Leu_{10}] intratumorally (left panels) and intravenously (right panels) injected in subcutaneous CT26 colorectal cancer bearing mice. Doxo equivalent doses of 2.4 mg/kg and 12 mg/kg were administered intratumorally and intravenously, respectively. A) and D): Animal body weight in the first three weeks following treatment (refer to supporting information for statistical comparison between different groups); B) and E): Tumor growth curves (refer to supporting information for statistical comparison between different groups); C) and F): Kaplan-Meier Survival curve. Results are expressed in mean ± SEM, $n = 6$–9; Statistical analysis of the treatments is referred to the untreated group: ***$p < 0.001$, **$p < 0.01$ *$p < 0.05$.

mouse model, also documented by the literature [40,59], did not allow for its use as a reference for the multiple administrations schedule.

Interestingly, 4T1 tumor bearing mice treated by IV with free Doxo exhibited significant body weight loss during the first two weeks compared to animals treated by single or multiple administration of $mPEG_{5kDa}$-b-[(Doxo-hydGlu)$_6$-*r*-Leu_{10}] (Fig. 8D; refer to supporting information for statistical comparison between different groups). Furthermore, significant lower body weight decrease was found after single and multiple injection of $mPEG_{5kDa}$-b-[(Doxo-hydGlu)$_6$-*r*-Leu_{10}] compared to the reference liposomal formulation Caelyx® administered at equivalent Doxo dose in single or multiple administrations, respectively.

Single or multiple intravenous administration of $mPEG_{5kDa}$-b-[(Doxo-hydGlu)$_6$-*r*-Leu_{10}] slowed down tumor growth compared to untreated mice (refer to supporting information for statistical comparison between different groups). Moreover, nearly overlapped tumor volume profiles found between $mPEG_{5kDa}$-b-[(Doxo-hydGlu)$_6$-*r*-Leu_{10}] (single or multiple injections) and Caelyx® multiple injections. Multiple $mPEG_{5kDa}$-b-[(Doxo-hydGlu)$_6$-*r*-Leu_{10}] injections show that the bioconjugate can be safely administered to achieve enhanced anticancer activity while limiting the toxicity of the drug. On the contrary, the Caelyx® formulation injected by a multiple administration regimen, caused a severe and irreversible body weight loss, highlighting its toxicity at this regimen and dose. Therefore, $mPEG_{5kDa}$-b-[(Doxo-hydGlu)$_6$-*r*-Leu_{10}] possesses a comparable therapeutic performance and a safer profile with respect to Caelyx®.

The median survival time increased after single or multiple $mPEG_{5kDa}$-(Doxo-hydGlu)$_6$-*r*-Leu_{10} administration and single Caelyx® administration with respect to the control untreated group ($p < 0.001$). The median survival was 35 and 37 days for single administration of $mPEG_{5kDa}$-(Doxo-hydGlu)$_6$-*r*-Leu_{10} and Caelyx®, respectively, compared to 27 days for untreated mice (Fig. 8E). On the contrary, single free Doxo administration and multiple Caelyx® administration dramatically reduced the survival rate. Overall, no significant survival difference was observed between single and weekly injections of $mPEG_{5kDa}$-b-[(Doxo-hydGlu)$_6$-*r*-Leu_{10}], which can be ascribed to the appearance of metastasis-related side effects that required the mouse sacrifice regardless of the tumor volumes. Indeed, the aggressiveness of this tumor model does not allow for long-term endpoint.

With the aim to investigate the tolerability of the polymer-based drug carrier a safety study was undertaken. *In vitro* studies showed that $mPEG_{5kDa}$-b-[(Doxo-hydGlu)$_6$-*r*-Leu_{10}] polymeric micelles induced

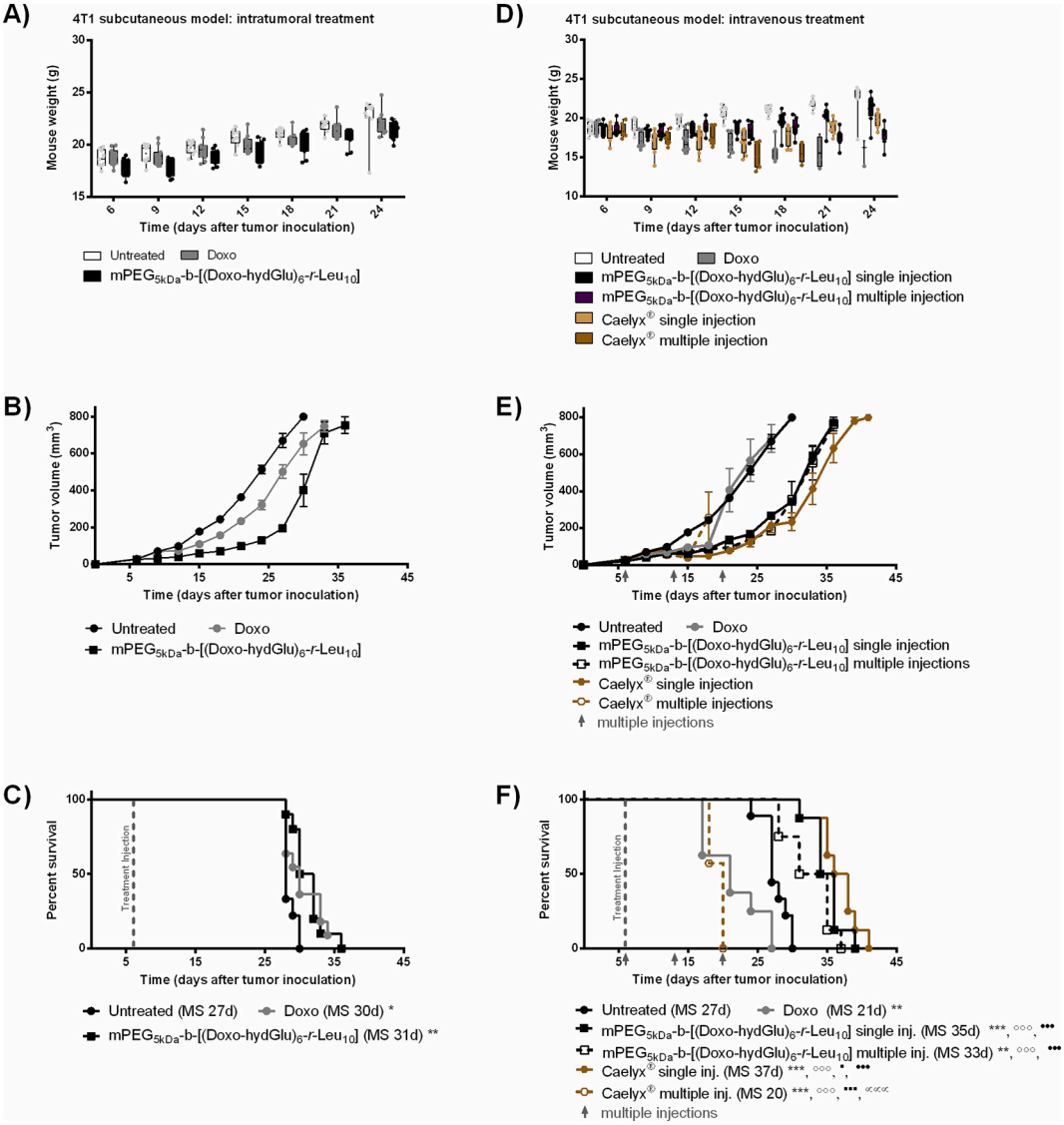

Fig. 8. *In vivo* antitumor efficacy of mPEG$_{5kDa}$-b-[(Doxo-hydGlu)$_6$-*r*-Leu$_{10}$] intratumorally (A, B, C) and intravenously (D, E, F) injected in subcutaneous 4T1 breast cancer bearing mice. Doxo equivalent doses of 3 mg/kg and 15 mg/kg were administered intratumorally and intravenously, respectively. Animal body weight in the first three weeks following treatment (A and D; refer to supporting information for statistical comparison between different groups); tumor growth curves (B and E; refer to supporting information for statistical comparison between different groups); Kaplan-Meier Survival curve (C and F) after administration of single (A, B, C) or single and weekly (D, E, F) (see arrows on "time" axis) administration of Doxo and mPEG$_{5kDa}$-b-[(Doxo-hydGlu)$_6$-r-Leu$_{10}$]. Caelyx® was also injected intravenously as control (D, E, F). Results are expressed in mean ± SEM, $n = 8$–11. A, B, C: For panels C and F, statistical analysis is referred to untreated group (*), Doxo (○), Caelyx® multiple injections (●), mPEG$_{5kDa}$-b-[(Doxo-hydGlu)$_6$-r-Leu$_{10}$] single injection (∝), mPEG$_{5kDa}$-b-[(Doxo-hydGlu)$_6$-r-Leu$_{10}$] multiple injections (■); triple marks: $p < 0.001$, double marks: $p < 0.01$, single mark: $p < 0.05$.

less than 4.5%, haemolysis (Fig. SI-25), which is the threshold for a haemolytic reaction [64]. After i.v. administration to mice, the blood analysis (Table SI-3) showed that mPEG$_{5kDa}$-b-[(Doxo-hydGlu)$_6$-*r*-Leu$_{10}$] did not significantly increase the levels of blood markers for organ toxicity, AST, BUN and CPK, while a slight increase of ALT and LDH was observed in comparison to untreated mice. On the contrary, Caelyx® significantly increased all marker levels except BUN, which suggests that the polymeric micelles are significantly safer to liver and heart than Caelyx®. Histologic analyses (Fig. SI-26) showed that the polymeric carrier has lower cardiac toxicity with respect to the reference Caelyx®, without induction of mononuclear cell infiltration and fibrosis. Hepatocytic cytoplasmic hydropic lesions were also less frequent and severe in mice treated with polymeric micelles than Caelyx®. Overall, the polymeric micelles showed a safer profile with respect to Caelyx® of which toxicity is extensively documented in the literature [65–69].

It should be noted that the main objective of this study was to evaluate the proof of concept of mPEG$_{5kDa}$-b-[(Doxo-hydGlu)$_m$-*r*-Leu$_n$] *co*-polymers as Doxo delivery systems for cancer treatment. For this reason, we chose to perform an anti-tumor efficacy study on two different subcutaneous tumor models. Considering the preliminary results obtained in this work, further studies will be carried out to evaluate the biodistribution and anticancer efficacy on orthotopic models.

4. Conclusions

The results obtained in this work show that the identification of the requisites allow for the rational design of PEG-polyaminoacid composition yielding *co*-polymers with optimized anticancer drug conjugation that self-assemble into colloidal nanocarriers and release the drug under controlled conditions. The introduction of leucine as spacer among the glutamic monomers minimizes steric hindrance that prevents complete co-polymer derivatization with drugs, and modulates the amphiphilicity

of the conjugate, which contributes to its self-assembly. Therefore, according to the physicochemical properties of the conjugated drug, suitable Glu/Leu molar ratio must be selected to compromise a high derivatization efficiency of the Glu monomers with drug and the increased hydrophobicity of the polyaminoacid block due to Leu, which contributes to the colloidal stability of the assembled materials.

In the case of Doxo (543.5 Da and 1.27 logP), the co-polymer including 6 hydGlu and 10 Leu [PEG_{5kDa}-b-($hydGlu_6$-*r*-Leu_{10})] was found to yield a drug conjugate with the best physicochemical and biopharmaceutical properties, drug loading, particle size, self-association, stability, and site selective controlled drug release. The resulting conjugate displayed excellent pharmaceutical performance by enhancing the selective anticancer activity of Doxo and significantly limiting its toxic side-effects, which provides for remarkably better therapeutic outcome in term of survival with respect to the parent drug Doxo. Furthermore, it may also offer a higher safety with respect to commercial colloidal systems designed to deliver Doxo.

The outcome of the systematic investigation we performed to select the most promising co-polymer can be exploited as background to generate other materials based on mixed polyaminoacid by introducing semisynthetic hydrophobic aminoacids as alternative to leucine that can modulate the self-assembling behavior of the amphiphilic co-polymer, the stability of the resulting colloidal carrier, the monomer conjugation efficiency with drug for pH-controlled release and that can, in addition, be exploited for physical encapsulation of anticancer drugs with poor aqueous solubility thus offering new opportunities for combination therapies.

Acknowledgement

This work was supported by the Italian Ministry of Education, University and Research (MIUR) through the "Progetti di ricerca di Rilevante Interesse Nazionale" (PRIN) scheme (MIUR grant code: 20175XBSX4).

Appendix A. Supplementary data

Supplementary data to this article can be found online at https://doi.org/10.1016/j.jconrel.2021.05.010.

References

[1] W.-l. Ye, J.-b. Du, R. Na, Y.-f. Song, Q.-b. Mei, M.-g. Zhao, S.-y. Zhou, Cellular uptake and antitumor activity of DOX-hyd-PEG-FA nanoparticles, PLoS One 9 (2014), e97358.
[2] C. LoPresti, H. Lomas, M. Massignani, T. Smart, G. Battaglia, Polymersomes: nature inspired nanometer sized compartments, J. Mater. Chem. 19 (2009) 3576–3590.
[3] K. Miyata, R.J. Christie, K. Kataoka, Polymeric micelles for nano-scale drug delivery, React. Funct. Polym. 71 (2011) 227–234.
[4] N. Zhao, M.C. Woodle, A.J. Mixson, Advances in delivery systems for doxorubicin, J. Nanomed. Nanotechnol. 9 (2018).
[5] H. Xu, Q. Yao, C. Cai, J. Gou, Y. Zhang, H. Zhong, X. Tang, Amphiphilic poly (amino acid) based micelles applied to drug delivery: the in vitro and in vivo challenges and the corresponding potential strategies, J. Control. Release 199 (2015) 84–97.
[6] A. Ponta, Y. Bae, PEG-poly (amino acid) block copolymer micelles for tunable drug release, Pharm. Res. 27 (2010) 2330–2342.
[7] E. Bernabeu, M. Cagel, E. Lagomarsino, M. Moretton, D.A. Chiappetta, Paclitaxel: what has been done and the challenges remain ahead, Int. J. Pharm. 526 (2017) 474–495.
[8] H. Maeda, J. Wu, T. Sawa, Y. Matsumura, K. Hori, Tumor vascular permeability and the EPR effect in macromolecular therapeutics: a review, J. Control. Release 65 (2000) 271–284.
[9] K.N. Sill, B. Sullivan, A. Carie, J.E. Semple, Synthesis and characterization of micelle-forming PEG-poly (amino acid) copolymers with iron-hydroxamate cross-linkable blocks for encapsulation and release of hydrophobic drugs, Biomacromolecules 18 (2017) 1874–1884.
[10] H. Cabral, K. Miyata, K. Osada, K. Kataoka, Block copolymer micelles in nanomedicine applications, Chem. Rev. 118 (2018) 6844–6892.
[11] Y. Bae, W.-D. Jang, N. Nishiyama, S. Fukushima, K. Kataoka, Multifunctional polymeric micelles with folate-mediated cancer cell targeting and pH-triggered drug releasing properties for active intracellular drug delivery, Mol. BioSyst. 1 (2005) 242–250.
[12] Y. Bae, N. Nishiyama, K. Kataoka, In vivo antitumor activity of the folate-conjugated pH-sensitive polymeric micelle selectively releasing adriamycin in the intracellular acidic compartments, Bioconjug. Chem. 18 (2007) 1131–1139.
[13] X. Yang, J.J. Grailer, I.J. Rowland, A. Javadi, S.A. Hurley, V.Z. Matson, D. A. Steeber, S. Gong, Multifunctional stable and pH-responsive polymer vesicles formed by heterofunctional triblock copolymer for targeted anticancer drug delivery and ultrasensitive MR imaging, ACS Nano 4 (2010) 6805–6817.
[14] R.B. Weiss, G. Sarosy, K. Clagett-Carr, M. Russo, B. Leyland-Jones, Anthracycline analogs the past, present, and future, Cancer Chemother. Pharmacol. 18 (1986) 185–197.
[15] P. Markland, G.L. Amidon, V.C. Yang, Modified polypeptides containing γ-benzyl glutamic acid as drug delivery platforms, Int. J. Pharm. 178 (1999) 183–192.
[16] A.J. Williams, V.K. Gupta, Self-assembly of a rodlike polypeptide on solid surfaces: role of solvent, molecular weight, and time of assembly, J. Phys. Chem. B 105 (2001) 5223–5230.
[17] N.M.B. Smeets, P.L.J. Van Der Weide, J. Meuldijk, J. Vekemans, L.A. Hulshof, A scalable synthesis of l-Leucine-N-carboxyanhydride, Org. Process. Res. Dev. 9 (2005) 757–763.
[18] W. Zhao, Y. Gnanou, N. Hadjichristidis, Fast and living ring-opening polymerization of α-amino acid N-carboxyanhydrides triggered by an "alliance" of primary and secondary amines at room temperature, Biomacromolecules 16 (2015) 1352–1357.
[19] S.L. Snyder, P.Z. Sobocinski, An improved 2, 4, 6-trinitrobenzenesulfonic acid method for the determination of amines, Anal. Biochem. 64 (1975) 284–288.
[20] G.E.C. Sims, T.J. Snape, A method for the estimation of polyethylene glycol in plasma protein fractions, Anal. Biochem. 107 (1980) 60–63.
[21] E. Ambrosio, M. Barattin, S. Bersani, S. Shubber, S. Uddin, C.F. van der Walle, P. Caliceti, S. Salmaso, A novel combined strategy for the physical PEGylation of polypeptides, J. Control. Release 226 (2016) 35–46.
[22] L. Piñeiro, M. Novo, W. Al-Soufi, Fluorescence emission of pyrene in surfactant solutions, Adv. Colloid Interf. Sci. 215 (2015) 1–12.
[23] J. Aguiar, P. Carpena, J.A. Molina-Bolıvar, C.C. Ruiz, On the determination of the critical micelle concentration by the pyrene 1: 3 ratio method, J. Colloid Interface Sci. 258 (2003) 116–122.
[24] H.T.T. Duong, F. Hughes, S. Sagnella, M. Kavallaris, A. Macmillan, R. Whan, J. Hook, T.P. Davis, C. Boyer, Functionalizing biodegradable dextran scaffolds using living radical polymerization: new versatile nanoparticles for the delivery of therapeutic molecules, Mol. Pharm. 9 (2012) 3046–3061.
[25] M.B. Hansen, S.E. Nielsen, K. Berg, Re-examination and further development of a precise and rapid dye method for measuring cell growth/cell kill, J. Immunol. Methods 119 (1989) 203–210.
[26] C. Bastiancich, K. Vanvarenberg, B. Ucakar, M. Pitorre, G. Bastiat, F. Lagarce, V. Préat, F. Danhier, Lauroyl-gemcitabine-loaded lipid nanocapsule hydrogel for the treatment of glioblastoma, J. Control. Release 225 (2016) 283–293.
[27] C.J. Zeiss, D.M. Gatti, O. Toro-Salazar, C. Davis, C.M. Lutz, F. Spinale, T. Stearns, M.B. Furtado, G.A. Churchill, Doxorubicin-induced cardiotoxicity in Collaborative Cross (CC) mice recapitulates individual cardiotoxicity in humans, G3 (Bethesda, Md.) 9 (2019) 2637–2646.
[28] V.G. Desai, E.H. Herman, C.L. Moland, W.S. Branham, S.M. Lewis, K.J. Davis, N. I. George, T. Lee, S. Kerr, J.C. Fuscoe, Development of doxorubicin-induced chronic cardiotoxicity in the B6C3F1 mouse model, Toxicol. Appl. Pharmacol. 266 (2013) 109–121.
[29] V.G. Desai, C.K. Joshua, V. Vijay, C.L. Moland, E.H. Herman, T. Lee, T. Han, S. M. Lewis, K.J. Davis, L. Muskhelishvili, S. Kerr, J.C. Fuscoe, Early biomarkers of doxorubicin-induced heart injury in a mouse model, Toxicol. Appl. Pharmacol. 281 (2014) 221–229.
[30] W.J. Reagan, M. York, B. Berridge, E. Schultze, D. Walker, S. Pettit, Comparison of cardiac troponin I and T, including the evaluation of an ultrasensitive assay, as indicators of doxorubicin-induced cardiotoxicity, Toxicol. Pathol. 41 (2013) 1146–1158.
[31] C. Deng, J. Wu, R. Cheng, F. Meng, H.-A. Klok, Z. Zhong, Functional polypeptide and hybrid materials: precision synthesis via α-amino acid N-carboxyanhydride polymerization and emerging biomedical applications, Prog. Polym. Sci. 39 (2014) 330–364.
[32] Y. Bae, S. Fukushima, A. Harada, K. Kataoka, Design of environment-sensitive supramolecular assemblies for intracellular drug delivery: polymeric micelles that are responsive to intracellular pH change, Angew. Chem. 115 (2003) 4788–4791.
[33] S.S. Banerjee, N. Aher, R. Patil, J. Khandare, Poly (ethylene glycol)-prodrug conjugates: concept, design, and applications, J. Drug Deliv. 2012 (2012) 103973.
[34] A.M. Eckman, E. Tsakalozou, N.Y. Kang, A. Ponta, Y. Bae, Drug release patterns and cytotoxicity of PEG-poly (aspartate) block copolymer micelles in cancer cells, Pharm. Res. 29 (2012) 1755–1767.
[35] Z. Amoozgar, Y. Yeo, Recent advances in stealth coating of nanoparticle drug delivery systems, in: Wiley Interdisciplinary Reviews: Nanomedicine and Nanobiotechnology 4, 2012, pp. 219–233.
[36] A. Dondoni, The emergence of thiol–ene coupling as a click process for materials and bioorganic chemistry, Angew. Chem. Int. Ed. 47 (2008) 8995–8997.
[37] X. Zhang, W. Tang, Z. Yang, X. Luo, H. Luo, D. Gao, Y. Chen, Q. Jiang, J. Liu, Z. Jiang, PEGylated poly (amine-co-ester) micelles as biodegradable non-viral gene vectors with enhanced stability, reduced toxicity and higher in vivo transfection efficacy, J. Mater. Chem. B 2 (2014) 4034–4044.
[38] J. Vega, S. Ke, Z. Fan, S. Wallace, C. Charsangavej, C. Li, Targeting doxorubicin to epidermal growth factor receptors by site-specific conjugation of C225 to poly (L-glutamic acid) through a polyethylene glycol spacer, Pharm. Res. 20 (2003) 826–832.

[39] V. Pliška, M. Schmidt, J.-L. Fauchère, Partition coefficients of amino acids and hydrophobic parameters π of their side-chains as measured by thin-layer chromatography, J. Chromatogr. A 216 (1981) 79–92.
[40] Y. Bae, N. Nishiyama, S. Fukushima, H. Koyama, M. Yasuhiro, K. Kataoka, Preparation and biological characterization of polymeric micelle drug carriers with intracellular pH-triggered drug release property: tumor permeability, controlled subcellular drug distribution, and enhanced in vivo antitumor efficacy, Bioconjug. Chem. 16 (2005) 122–130.
[41] Y. Bae, K. Kataoka, Intelligent polymeric micelles from functional poly (ethylene glycol)-poly (amino acid) block copolymers, Adv. Drug Deliv. Rev. 61 (2009) 768–784.
[42] O. Zagorodko, J.J. Arroyo-Crespo, V.J. Nebot, M.J. Vicent, Polypeptide-based conjugates as therapeutics: opportunities and challenges, Macromol. Biosci. 17 (2017) 1600316.
[43] S.C. Owen, D.P.Y. Chan, M.S. Shoichet, Polymeric micelle stability, Nano Today 7 (2012) 53–65.
[44] H. Phan, R.I. Minut, P. McCrorie, C. Vasey, R.R. Larder, E. Krumins, M. Marlow, R. Rahman, C. Alexander, V. Taresco, A.K. Pearce, Role of Self-Assembly Conditions and Amphiphilic Balance on Nanoparticle Formation of PEG-PDLLA Copolymers in Aqueous Environments 57, 2019, pp. 1801–1810.
[45] F. Danhier, O. Feron, V. Préat, To exploit the tumor microenvironment: passive and active tumor targeting of nanocarriers for anti-cancer drug delivery, J. Control. Release 148 (2010) 135–146.
[46] Y. Matsumura, H. Maeda, A new concept for macromolecular therapeutics in cancer chemotherapy: mechanism of tumoritropic accumulation of proteins and the antitumor agent smancs, Cancer Res. 46 (1986) 6387–6392.
[47] V. Torchilin, Tumor delivery of macromolecular drugs based on the EPR effect, Adv. Drug Deliv. Rev. 63 (2011) 131–135.
[48] S. Raddatz, J. Mueller-Ibeler, J. Kluge, L. Wäß, G. Burdinski, J.R. Havens, T. J. Onofrey, D. Wang, M. Schweitzer, Hydrazide oligonucleotides: new chemical modification for chip array attachment and conjugation, Nucleic Acids Res. 30 (2002) 4793–4802.
[49] M. Li, W. Song, Z. Tang, S. Lv, L. Lin, H. Sun, Q. Li, Y. Yang, H. Hong, X. Chen, Nanoscaled poly (L-glutamic acid)/doxorubicin-amphiphile complex as pH-responsive drug delivery system for effective treatment of nonsmall cell lung cancer, ACS Appl. Mater. Interfaces 5 (2013) 1781–1792.
[50] S. Salmaso, A. Semenzato, S. Bersani, F. Mastrotto, A. Scomparin, P. Caliceti, Site-selective protein glycation and PEGylation, Eur. Polym. J. 44 (2008) 1378–1389.
[51] J.J. Arroyo-Crespo, A. Armiñán, D. Charbonnier, L. Balzano-Nogueira, F. Huertas-López, C. Martí, S. Tarazona, J. Forteza, A. Conesa, M.J. Vicent, Tumor microenvironment-targeted poly-L-glutamic acid-based combination conjugate for enhanced triple negative breast cancer treatment, Biomaterials 186 (2018) 8–21.
[52] F. Danhier, T.T.B. Kouhé, N. Duhem, B. Ucakar, A. Staub, N. Draoui, O. Feron, V. Préat, Vitamin E-based micelles enhance the anticancer activity of doxorubicin, Int. J. Pharm. 476 (2014) 9–15.
[53] X. Gao, B. Wang, X. Wei, W. Rao, F. Ai, F. Zhao, K. Men, B. Yang, X. Liu, M. Huang, Preparation, characterization and application of star-shaped PCL/PEG micelles for the delivery of doxorubicin in the treatment of colon cancer, Int. J. Nanomedicine 8 (2013) 971–982.
[54] C.J. Lovitt, T.B. Shelper, V.M. Avery, Doxorubicin resistance in breast cancer cells is mediated by extracellular matrix proteins, BMC Cancer 18 (2018) 41.
[55] E. Markovsky, H. Baabur-Cohen, R. Satchi-Fainaro, Anticancer polymeric nanomedicine bearing synergistic drug combination is superior to a mixture of individually-conjugated drugs, J. Control. Release 187 (2014) 145–157.
[56] A. Balasso, S. Salmaso, P. Pontisso, A. Rosato, S. Quarta, A. Malfanti, F. Mastrotto, P. Caliceti, Re-programming pullulan for targeting and controlled release of doxorubicin to the hepatocellular carcinoma cells, Eur. J. Pharm. Sci. 103 (2017) 104–115.
[57] U. Beyer, T. Roth, P. Schumacher, G. Maier, A. Unold, A.W. Frahm, H.H. Fiebig, C. Unger, F. Kratz, Synthesis and in vitro efficacy of transferrin conjugates of the anticancer drug chlorambucil, J. Med. Chem. 41 (1998) 2701–2708.
[58] L.P. Belnap, P.H. Cleveland, M.E.M. Colmerauer, R.M. Barone, Y.H. Pilch, Immunogenicity of chemically induced murine colon cancers, Cancer Res. 39 (1979) 1174–1179.
[59] S. Lv, M. Li, Z. Tang, W. Song, H. Sun, H. Liu, X. Chen, Doxorubicin-loaded amphiphilic polypeptide-based nanoparticles as an efficient drug delivery system for cancer therapy, Acta Biomater. 9 (2013) 9330–9342.
[60] C.Y.X. Chua, J. Ho, S. Demaria, M. Ferrari, A. Grattoni, Emerging Technologies for Local Cancer Treatment 3, 2020, p. 2000027.
[61] B.A. Pulaski, S. Ostrand-Rosenberg, Mouse 4T1 breast tumor model, Curr. Protoc. Immunol. 39 (2000) 20–22.
[62] T. Tejada-Berges, C.O. Granai, M. Gordinier, W. Gajewski, Caelyx/Doxil for the treatment of metastatic ovarian and breast cancer, Expert. Rev. Anticancer. Ther. 2 (2002) 143–150.
[63] M.E.R. O'Brien, N. Wigler, M. Inbar, R. Rosso, E. Grischke, A. Santoro, R. Catane, D.G. Kieback, P. Tomczak, S.P. Ackland, Reduced cardiotoxicity and comparable efficacy in a phase III trial of pegylated liposomal doxorubicin HCl (CAELYXTM/Doxil®) versus conventional doxorubicin for first-line treatment of metastatic breast cancer, Ann. Oncol. 15 (2004) 440–449.
[64] M. Rahimi, K.D. Safa, E. Alizadeh, R. Salehi, Dendritic chitosan as a magnetic and biocompatible nanocarrier for the simultaneous delivery of doxorubicin and methotrexate to MCF-7 cell line, New J. Chem. 41 (2017) 3177–3189.
[65] A. Maksimenko, F. Dosio, J. Mougin, A. Ferrero, S. Wack, L.H. Reddy, A.A. Weyn, E. Lepeltier, C. Bourgaux, B. Stella, L. Cattel, P. Couvreur, A unique squalenoylated and nonpegylated doxorubicin nanomedicine with systemic long-circulating properties and anticancer activity, Proc. Natl. Acad. Sci. U. S. A. 111 (2014) E217–E226.
[66] F.A. Boratto, M.S. Franco, A.L.B. Barros, G.D. Cassali, A. Malachias, L.A. M. Ferreira, E.A. Leite, Alpha-tocopheryl succinate improves encapsulation, pH-sensitivity, antitumor activity and reduces toxicity of doxorubicin-loaded liposomes, Eur. J. Pharm. Sci. 144 (2020) 105205.
[67] C. Stark, P. Taimen, T. Savunen, J. Koskenvuo, Pegylated and liposomal doxorubicin is associated with high mortality and causes limited cardiotoxicity in mice, BMC Res. Notes 11 (2018) 148.
[68] R. Zhang, Y. Zhang, Y. Zhang, X. Wang, X. Gao, Y. Liu, X. Zhang, Z. He, D. Wang, Y. Wang, Ratiometric delivery of doxorubicin and berberine by liposome enables superior therapeutic index than Doxil®, Asian J. Pharm. Sci. 15 (2020) 385–396.
[69] T. Safra, F. Muggia, S. Jeffers, D.D. Tsao-Wei, S. Groshen, O. Lyass, R. Henderson, G. Berry, A. Gabizon, Pegylated liposomal doxorubicin (doxil): reduced clinical cardiotoxicity in patients reaching or exceeding cumulative doses of 500 mg/m2, Ann. Oncol. 11 (2000) 1029–1033.